Article

SOURCE DATA | TRANSPARENT PROCESS

EMBO reports

An LTR retrotransposon-derived lncRNA interacts with RNF169 to promote homologous recombination

Bing Deng†, Wenli Xu†, Zelin Wang, Chang Liu, Penghui Lin, Bin Li, Qiaojuan Huang, Jianhua Yang*, Hui Zhou** & Lianghu Qu***

Abstract

LTR retrotransposons are abundant repetitive elements in the human genome, but their functions remain poorly understood. Here, we report the function and regulatory mechanism of an ERV-9 LTR retrotransposon-derived lncRNA called p53-regulated lncRNA for homologous recombination (HR) repair 1 (PRLH1) in human cells. PRLH1 is highly expressed in p53-mutated hepatocellular carcinoma (HCC) samples and promotes cell proliferation in p53-mutated HCC cells, and its transcription is promoted by NF-Y and suppressed by p53. Mechanistically, PRLH1 specifically binds to an uncharacterized domain of RNF169 through two GCUUCA boxes in its 5′ terminal region to form a DNA repair complex that supplants 53BP1 at double-strand break (DSB) sites and then promotes the initiation of HR repair. Notably, PRLH1 is essential for the stabilization of RNF169, acting as an RNA platform to recruit and assemble HR protein factors. This study characterizes PRLH1 as a novel HR-promoting factor and provides new insights into the function and mechanism of LTR retrotransposon-derived lncRNAs.

Keywords HR repair; lncRNA; LTR retrotransposon; p53; RNF169
Subject Categories DNA Replication & Repair; RNA Biology
DOI 10.15252/embr.201847650 | Received 28 December 2018 | Revised 10 August 2019 | Accepted 14 August 2019 | Published online 5 September 2019
EMBO Reports (2019) 20: e47650

Introduction

DNA repair is an important biological process that maintains the integrity of genomic DNA and normal physiological functions such as cell division. Among the various types of DNA lesions, DSBs are the most harmful and difficult to repair [1,2]. Fortunately, cells have two major pathways to repair DSBs: nonhomologous end joining (NHEJ) and homologous recombination (HR). Since HR and NHEJ are two competitive pathways in the early period of DSB repair [3–5], alternative selection in a spatiotemporal-dependent manner or maintaining a proper balance between the two pathways is very important for cells to preserve genome stability [6,7]. The choice between HR and NHEJ is regulated by 53BP1, a p53-binding protein that antagonizes the resection of DSBs and favors NHEJ [8–10]. However, the newly discovered E3 ubiquitin ligase RNF169 can displace 53BP1 from the RNF8/RNF168-modified chromatin at DSB sites to promote the initiation of HR repair [11,12]. Since RNF169 has been proposed to have a higher affinity to these binding sites than 53BP1 [13], whether other HR components cooperate with RNF169 to achieve this pivotal function is required to be studied and this research aspect may be helpful to decipher the machinery and mechanism of HR-mediated DSB repair.

p53 is a very important tumor suppressor and one of the most frequently mutated genes in cancers [14,15]. In response to DNA damage, p53 can be activated and cause cell cycle arrest or apoptosis by transcriptionally regulating a series of protein genes and noncoding RNAs (ncRNAs) [16–19]. As a "guardian of the genome", p53 can suppress HR repair to maintain genome stability [20]. HR is the main error-free DNA repair approach and is required for cell division that involves sister chromatid exchanges, but both defective HR activity and exacerbated HR activity in cells contribute to genome instability and tumorigenesis [21–23]. Previous studies have shown that spontaneous and stress-induced HR is strictly inhibited by p53 through a direct interaction with some HR proteins [20,24–26] or transcriptional repression of Rad51 [27]. Recent studies have shown that lncRNAs are emerging as regulators of HR repair [28–30], but whether they are involved in the p53-mediated repression of HR pathway remains unexplored.

Retrotransposons including LINEs, SINEs and solitary long terminal repeats (LTRs) of human endogenous retroviruses (HERVs) comprise over 40% of the human genome DNA. Retrotransposons are transcriptional regulators capable of initiating RNA synthesis [31,32]. Specifically, LTR retrotransposons which contain the U3, R, U5 regions without retrovirus genes, often contain promoters and enhancers to regulate the transcription of many genes including

MOE Key Laboratory of Gene Function and Regulation, State Key Laboratory for Biocontrol, Sun Yat-sen University, Guangzhou, China
*Corresponding author. Tel: +86 20 84112399; Fax: +86 20 84036551; E-mail: yangjh7@mail.sysu.edu.cn
**Corresponding author. Tel: +86 20 84112399; Fax: +86 20 84036551; E-mail: lsszh@mail.sysu.edu.cn
***Corresponding author. Tel: +86 20 84112399; Fax: +86 20 84036551; E-mail: lssqlh@mail.sysu.edu.cn
† These authors contributed equally to this work

lncRNAs [33–35]. Several LTR families, such as LTR10 and MER61, are enriched for p53-binding sites [36], implying that p53 can activate the transcription of a large group of LTR retrotransposon-derived RNAs. More importantly, LTRs of a well-known ERV-9 family are bound by NF-Y, a partner of the p53 pathway, at the CCAAT motifs of the U3 region to effectively promote the expression of ERV-9 LTR lncRNAs, which can act in cis to regulate transcription of downstream genes [37,38]. Although these studies have shown the transcription and regulatory effect of LTR retrotransposon-derived lncRNAs, their roles in specific biological processes are still largely unknown.

In this study, we performed a systematical screen of lncRNA candidates from The Cancer Genome Atlas (TCGA) and identified an LTR retrotransposon-derived lncRNA PRLH1, the expression of which is promoted by NF-Y and suppressed by p53. We then conducted RNA–protein interaction assays and characterized the DNA repair protein RNF169 as a specific RNA-binding protein of PRLH1. Most interestingly, our investigation showed that PRLH1 played an important role in the formation of RNA–protein complex that promoted the HR-mediated DSB repair, and revealed the novel potential function of LTR retrotransposon-derived lncRNAs in cells.

Results

PRLH1 is an ERV-9 LTR lncRNA regulated by p53

To explore the p53-associated lncRNA candidates, a comparative analysis of the lncRNA expression in p53-mutated and wild-type HCC specimens was performed. We analyzed the RNA-seq data of 371 primary tumor and 50 normal samples from the TCGA project. Sixty-three lncRNAs were identified as differentially expressed lncRNAs in HCC tumors relative to those expressed in normal tissues (fold-change ≥ 8, FDR < 0.05; Fig 1A and Table EV1), and 44 lncRNAs were markedly and differentially expressed between the p53-mutated ($n = 61$) and wild-type HCC tumors ($n = 133$) (fold-change ≥ 4, FDR < 0.05; Fig 1B and Table EV1). The cross-comparison of the above two gene lists revealed an overlap of 10 lncRNAs, which were regarded as p53-related lncRNA candidates (Fig 1C). Among these candidates, lncRNA PRLH1, which was annotated as LINC01419 in the RefSeq gene sets, showed the largest upregulation in HCC tumors relative to that in normal tissues (~27-fold, Fig 1D). This result was consistent with a recent study that revealed higher expression of LINC01419 in a cohort of Chinese HCC patients compared to its expression in healthy people [39]. Importantly, we further showed an eightfold upregulation of PRLH1 expression in p53-mutated HCC samples compared to that in wild-type ones (Fig 1D), strongly suggesting a p53-repressed mechanism of PRLH1 expression.

The expression of PRLH1 was also analyzed in HCC cell lines with wild-type or mutated p53 gene backgrounds. Compared with the expression in immortalized human hepatocyte LO2 cells, PRLH1 expression was slightly lower in HepG2 cells with wild-type p53 but significantly higher in the other three HCC cell lines (SK-HEP-1, SMMC-7721, PLC/PRF/5, HuH-7). Notably, the PRLH1 expression in HuH-7 and PLC/PRF/5 cells, which contain mutant p53 proteins, was much higher than that in SK-HEP-1 and SMMC-7721 cells, which express wild-type p53 (Fig 1E). These results are in good agreement with the above results from TCGA data analysis.

To further identify the negative correlation between the expression of wild-type p53 and PRLH1, we knocked down or knocked out p53 expression in p53 wild-type and mutant cells using an siRNA or CRISPR/Cas9 system, respectively. As expected, we found that the expression of PRLH1 increased nearly up to eightfold in SK-HEP-1 cells, while remaining unchanged in HuH-7 cells after knockdown of p53 by siRNA (Fig 1F). Remarkably, the expression of PRLH1 was upregulated more than 30-fold in two HepG2-KO-p53 cell lines (#5, #6), which were made devoid of p53 protein using the CRISPR/Cas9 system (Appendix Fig S1A–F), compared with the expression in HepG2 wild-type cells (Fig 1G). Notably, the knockout of p53 in HepG2 cells led to a remarkable decrease in the expression of the known p53-activated lncRNA PURPL [40] and a significant increase in the expression of other three lncRNAs (AC073236.3, RP11-81H3.2, and RP11-328N19.1) displayed in Fig 1C (Appendix Fig S1G), indicating that these three lncRNAs were also repressed directly or indirectly by wild-type p53. These results suggest that the expression of PRLH1 is repressed by wild-type p53 but not mutant p53.

To confirm that PRLH1 is a genuine lncRNA without protein-coding ability, we used the prediction software, ORF finder (https://www.ncbi.nlm.nih.gov/orffinder/), to predict the putative ORFs in PRLH1, and then, the Western blot analysis of FLAG-tagged proteins showed that all three putative ORFs in PRLH1 had no coding ability (Fig EV1A). We also found that PRLH1 was distributed in both nuclear and cytoplasmic fractions of cells (Fig EV1B). To identify the full-length sequence of PRLH1, we performed 5′-RACE and 3′-RACE assays and found two PRLH1 isoforms with different lengths originated from alternative termination sites (Fig EV1C and D). Very interestingly, an LTR12C element, which belongs to the primate-specific ERV-9 LTR family [41], is located across the promoter and the first exon of PRLH1, indicating that PRLH1 is a member of the ERV-9 lncRNA family. The PRLH1 transcript also exists in gorilla and chimp, beside humans, and the sequence of it is highly conserved in these species (Fig EV1E). Altogether, we identified that PRLH1 was an ERV-9 LTR lncRNA and its expression was suppressed by p53.

The NF-Y transcription factor is required for the expression and p53-mediated repression of PRLH1

Given the findings that PRLH1 expression is repressed by wild-type p53 in HCC samples and cell lines, we further explored the mechanism underlying transcription and regulation of PRLH1. p53 has been reported to be able to directly repress the transcription of targeted genes through binding to the promoters or squelching transcription activators of the target genes [16]. Since no p53-binding was found in the PRLH1 promoter in our ChIP assay (Fig 2A), and in the updated ChIP-seq data from our ChIPBASE v2.0 database (http://rna.sysu.edu.cn/chipbase/) [42], which contains numerous cell lines and tissues, we moved to identify the important transcription activator for PRLH1.

Since the ERV-9 LTRs are usually bound by the transcription factor NF-Y at the CCAAT motifs to assemble a robust LTR enhancer complex [37,38], and the ChIP-seq data from the ChIPBASE v2.0 database showed that the NF-Y bound to the proximal promoter of PRLH1 in chronic myeloid leukemia K562 cells, we analyzed the promoter sequence of PRLH1 and found that there exist four CCAAT

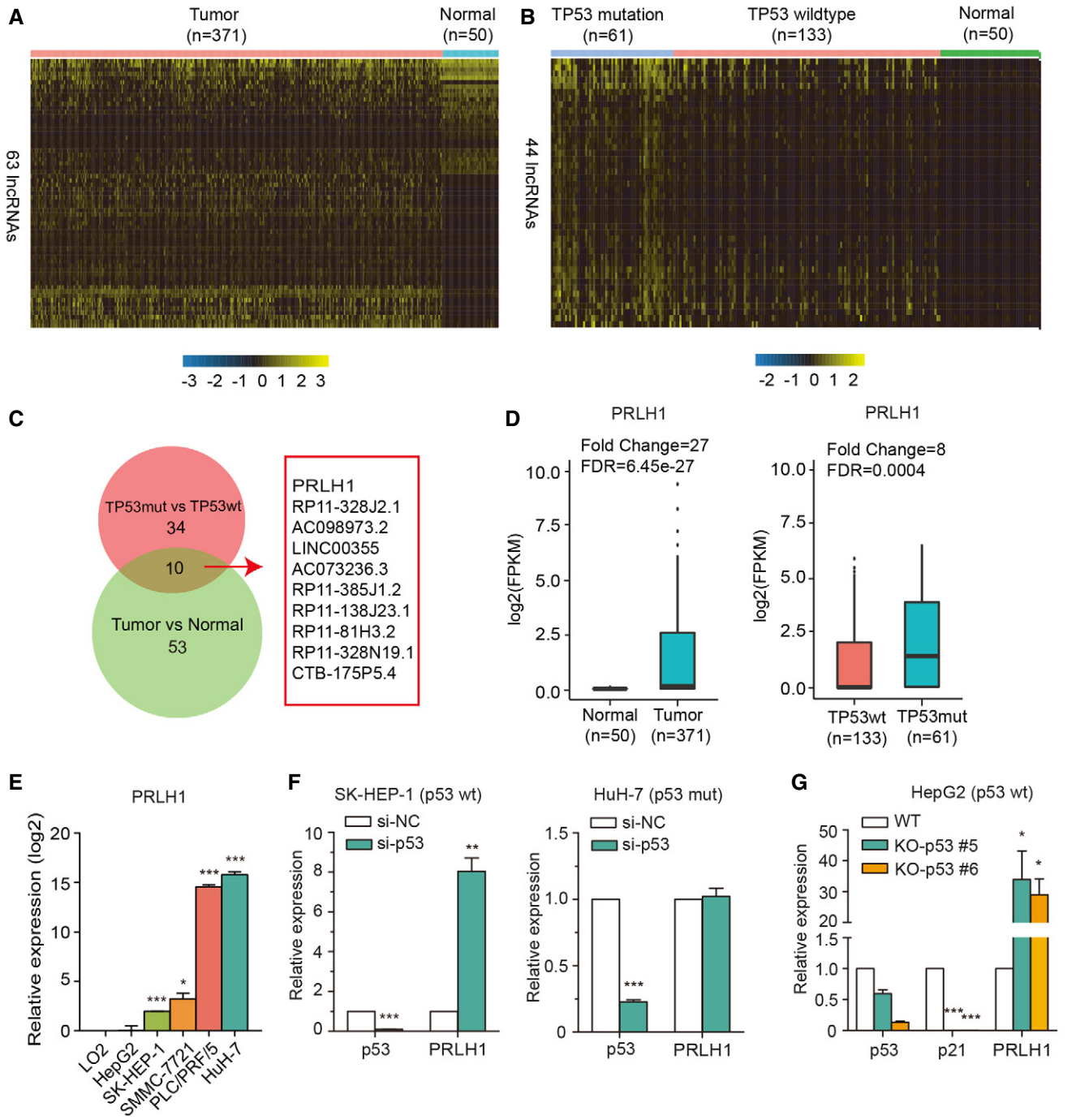

Figure 1. PRLH1 is regulated by p53.

A Heat map of lncRNAs with significantly differential expression between HCC tissues and normal tissues. The expression values were log10-transformed.

B Heat map of lncRNAs with significantly differential expression between p53-mutated and wild-type HCC samples. The expression values were log10-transformed.

C Venn plot showing an overlap of lncRNAs between the two groups above.

D Boxplots showing the PRLH1 expression in tumor and p53-mutated samples. Left, the sample numbers of the normal tissues and HCC tumor tissues were 50 and 371, respectively. Right, the numbers of p53 wild-type and mutated HCC samples were 133 and 61, respectively. In the boxplots, the horizontal bands within the boxes indicate the median, the box ranges mark the upper and lower quartiles, and the whiskers represent the maximum and minimum values excluding outliers, within 1.5 times of the interquartile range from the box.

E The relative expression of PRLH1 measured by qRT–PCR analyses in liver cancer cell lines.

F The relative expression of PRLH1 in SK-HEP-1 and HuH-7 cells transfected with p53 siRNA for 48 h, as determined by qRT–PCR analyses. The SK-HEP-1 and HuH-7 cells were p53-wild-type (wt) and p53-mutated (mut), respectively.

G The relative expression of PRLH1 measured by qRT–PCR analyses in HepG2 (p53-wt) and two HepG2-KO-p53 cell lines (#5 and #6).

Data information: In (E–G), error bars, SEM ($n = 3$ independent cell cultures). *$P < 0.05$; **$P < 0.01$; and ***$P < 0.001$ by two-tailed paired Student's t-test.

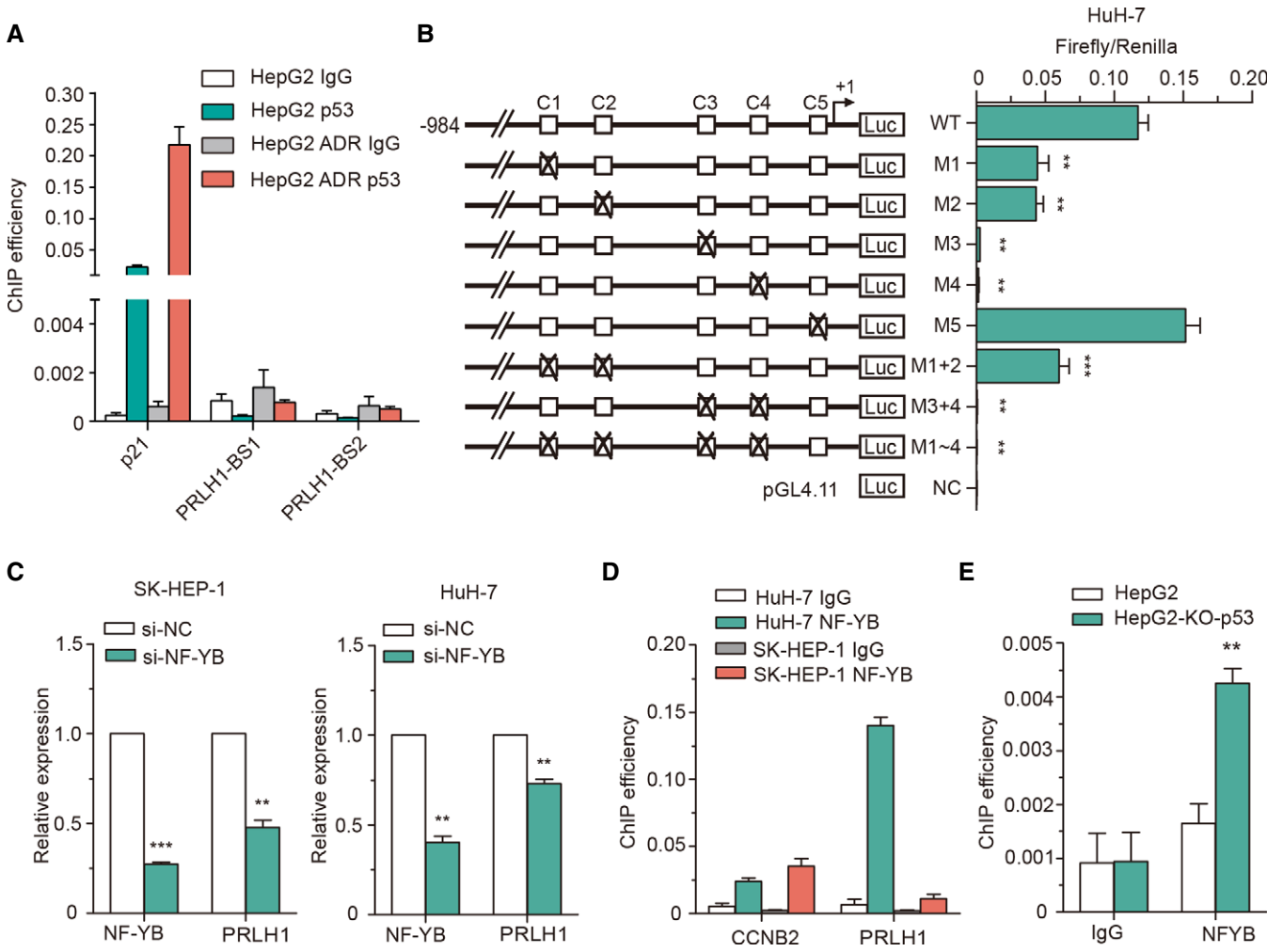

Figure 2. NF-Y is the transcription factor of PRLH1, and its binding to the PRLH1 promoter is repressed by p53.

A ChIP efficiencies of p53 detected by qPCR. The primers were specific to the potential p53-binding sites in the PRLH1 promoter (BS1, BS2). The assay was performed using the cell lysates derived from HepG2 cells treated with 500 ng/ml ADR for 48 h or without treatment, using p21 as a positive control gene and IgG as a negative control antibody. The values of ChIP efficiencies are given as % of input.

B The luciferase reporter assays measuring the promoter activity with the PRLH1 promoter–reporter vectors containing the wild-type or mutant CCAAT motifs in HuH-7 cells. The pGL4.11 vector was used as a negative control. The schematic of the reporter vectors is shown on the left. Open boxes (C1 to C5) represent wild-type CCAAT motifs, and crossed boxes represent the corresponding mutant CCAAT motifs.

C The relative expression of NF-YB and PRLH1 in SK-HEP-1 and HuH-7 cells transfected with NF-YB siRNA for 48 h, as determined by qRT–PCR assays.

D ChIP efficiencies showing the amount of PRLH1 promoter bound to NF-YB in SK-HEP-1 and HuH-7 cells by qPCR analyses. CCNB2 was used as a positive control gene and IgG as a negative control antibody. The values of ChIP efficiencies are given as % of input with SEM indicated.

E ChIP efficiencies showing the amount of PRLH1 promoter bound to NF-YB in HepG2 and HepG2-KO-p53 cells by qPCR analyses.

Data information: Error bars, SEM ($n = 3$ independent cell cultures). *$P < 0.05$; **$P < 0.01$; and ***$P < 0.001$ by two-tailed paired Student's t-test.

boxes and a putative reversed box with ATTGG located within 300 bp from the transcription initiation site (Appendix Fig S2). To determine whether these motifs can have an activation effect on the transcription of PRLH1, luciferase assays were performed using pGL4.11 promoter–reporter vectors, which contained the wild-type or CCAAT-mutant PRLH1 promoter in HuH-7 cells (Fig 2B and Appendix Fig S2). Compared with the activities of the wild-type promoter, the promoter activities of the M3 or M4 promoters were more than 80% decreased, those of the M1 or M2 promoters were nearly 50% decreased, and the vector containing the first four mutant CCAAT boxes (M1~4) had almost no promoter activity. However, the promoter activity of the M5 promoter was not significantly different from that of the wild-type promoter. These results suggest that the PRLH1 promoter is substantially activated by the first four CCAAT boxes, especially C3 and C4 (Fig 2B). To further evaluate the involvement of NF-Y in the transcriptional activation of PRLH1, NF-YB expression was knocked down by siRNAs in SK-HEP-1 and HuH-7 cells. qRT–PCR analysis revealed that the expression of PRLH1 in both cells was markedly decreased (Fig 2C).

Moreover, chromatin immunoprecipitation (ChIP) was used to investigate whether NF-Y can be effectively recruited to the promoter of PRLH1. As shown in Fig 2D, in line with the positive

control gene CCNB2, the promoter fragment of PRLH1 containing the first four CCAAT boxes was specifically amplified from the immunoprecipitate with an antibody against NF-YB but not with a control IgG antibody, strongly suggesting that NF-Y is the important transcription activator for PRLH1. Notably, the results showed that the combination of the NF-Y complex and the PRLH1 promoter was very strong in the mutant p53 cell line HuH-7 but weak in the wild-type p53 cell line SK-HEP-1 (Fig 2D), in agreement with the expression level of PRLH1 in these two cell lines.

p53 is well known to be able to repress the transcription of genes, in many cases by preventing the binding of the NF-Y transcription factor to their promoters [43–47]. We assumed that PRLH1 transcription might also be regulated by p53 in the same manner because, in this study, the suppression of PRLH1 expression was tightly correlated with the expression of wild-type p53. To validate this hypothesis, ChIP assays were performed in HepG2 and HepG2-KO-p53 cells. As expected, the binding of NF-Y to the PRLH1 promoter in HepG2 was very weak, but their binding in the HepG2-KO-p53 cells was significantly higher than that in HepG2 cells (Fig 2E). Together, these results revealed that PRLH1 was transactivated by the NF-Y transcription factor, and p53 repressed the transcription of PRLH1 by preventing the binding of NF-Y to the PRLH1 promoter.

PRLH1 promotes proliferation of the p53-mutated HCC cell lines

Since PRLH1 was significantly upregulated in p53-mutated HCC samples and cell lines, we wondered whether PRLH1 was involved in p53-related biological processes. We first estimated the relationship between PRLH1 and the differentially expressed protein-coding genes in the TCGA data sets of HCC based on co-expression profiles of genes, and then performed a Gene Ontology (GO) analysis using the protein-coding genes positively related to PRLH1. The result showed that these genes presented significant enrichments in cell division, DNA replication, and DNA repair (FDR < 0.05, Fig 3A), indicating that PRLH1 may be involved in the processes of cell proliferation.

To validate this possibility, we performed Cell Counting Kit-8 (CCK-8) and colony formation assays in the HuH-7 cell line after knockdown or overexpression of PRLH1. As expected, we found that the knockdown of PRLH1 expression using RNAi and CRISPRi methods significantly impaired the proliferation ability of the HuH-7 cells (Fig 3B–E). We also observed a significant decrease of cell growth ability in PLC/PRF/5 transfected with PRLH1 siRNA (Fig EV2A and B). In contrast, in both CCK-8 and colony formation assays, HuH-7 and PLC/PRF/5 cells overexpressing PRLH1 showed higher proliferation rates than cells transfected with the empty vector (Figs 3F–H and EV2C and D). Intriguingly, we also overexpressed PRLH1 in two p53 wild-type HCC cell lines (SK-HEP-1 and HepG2), but no significant increase in cell growth ability was achieved in the CCK-8 assay in either of the cell lines (Fig EV2E and F). Knockdown of PRLH1 using RNAi or CRISPRi methods in HepG2 cells also had no significant effect on cell proliferation (Fig EV2G and H). All these results confirm that PRLH1 can promote cell proliferation of mutated p53 HCC cells but not wild-type p53 HCC cells, indicating that the function of PRLH1 may be tightly related to the p53 or p53-regulated network.

PRLH1 specifically binds to the DNA repair protein RNF169

To further investigate the biological function and mechanism of PRLH1 in cells, we performed an RNA pull-down assay followed by mass spectrometry (MS) analysis to identify the proteins associated with PRLH1 (Fig 4A). The MS analysis of the protein band specific to PRLH1 RNA revealed that RNF169 specifically bound to PRLH1 with the highest and most significant score among 10 detected proteins (Fig 4B and Appendix Table S1). RNF169 is an E3 ubiquitin ligase that has been reported as a negative regulator of the ubiquitin-dependent DNA damage signaling cascade and is involved in HR-mediated DNA repair [11,48,49].

To verify the association between RNF169 and PRLH1, Western blot analysis with the RNF169 antibody was performed. The result revealed that RNF169 was enriched in the PRLH1 pull-down protein samples but not in proteins associated with antisense PRLH1 (Fig 4C). Furthermore, we carried out native RNA immunoprecipitation (RIP) assays to confirm the binding of PRLH1 to the RNF169 protein. The RIP assays with the FLAG antibody on cellular extracts of HuH-7 cells overexpressing FLAG-RNF169 showed that there was a significantly higher enrichment of PRLH1 with FLAG than those assays with the IgG control antibody (Figs 4D and EV3A–C). The results of the native RIP and UV-crossed RIP assays using the RNF169 antibody showed that PRLH1 could specifically bind to the endogenous RNF169 protein (Figs 4E and EV3D). Furthermore, we performed tRSA RNA pull-down assays in HuH-7 cells and the result showed that both of the PRLH1 transcripts could specifically bind to RNF169, but not RNF168 (Fig EV3E). We also predicted the correlation between PRLH1 and RNF169 using the catRAPID system [50] and found that it was up to 99%. Together, these results strongly suggest that PRLH1 specifically interacts with RNF169 protein.

Figure 3. PRLH1 promotes cell proliferation in HuH-7 cells.

A The enrichment of the protein-coding genes with a positive correlation with PRLH1 in GO terms (Pearson's $r > 0.2$).

B The relative expression of PRLH1 determined by qRT–PCR in HuH-7 cells (left) transfected with si-NC or si-PRLH1 and in HuH-7-KRAB cells (right) transfected with two sgRNAs for PRLH1 (sg-1 and sg-2) or a control sgRNA (sg-Lacz).

C–E CCK-8 assays (C) and colony formation assays (D, E) showing the cell viability after PRLH1 knockdown in HuH-7 cells and HuH-7-KRAB cells.

F The relative expression of PRLH1 determined by qRT–PCR in HuH-7 cells transfected with pcDNA3.0 empty vector or two pcDNA3.0-PRLH1 vectors (PRLH1-1 and PRLH1-2).

G CCK-8 assays showing the cell viability in pcDNA3.0- and pcDNA3.0-PRLH1-transfected HuH-7 cells.

H Colony formation assays showing the cell viability in HuH-7 cells overexpressing PRLH1.

Data information: In (B–H), the experiments were performed in three biological replicates. Error bars, SEM $*P < 0.05$; $**P < 0.01$; and $***P < 0.001$ by two-tailed paired Student's *t*-test.

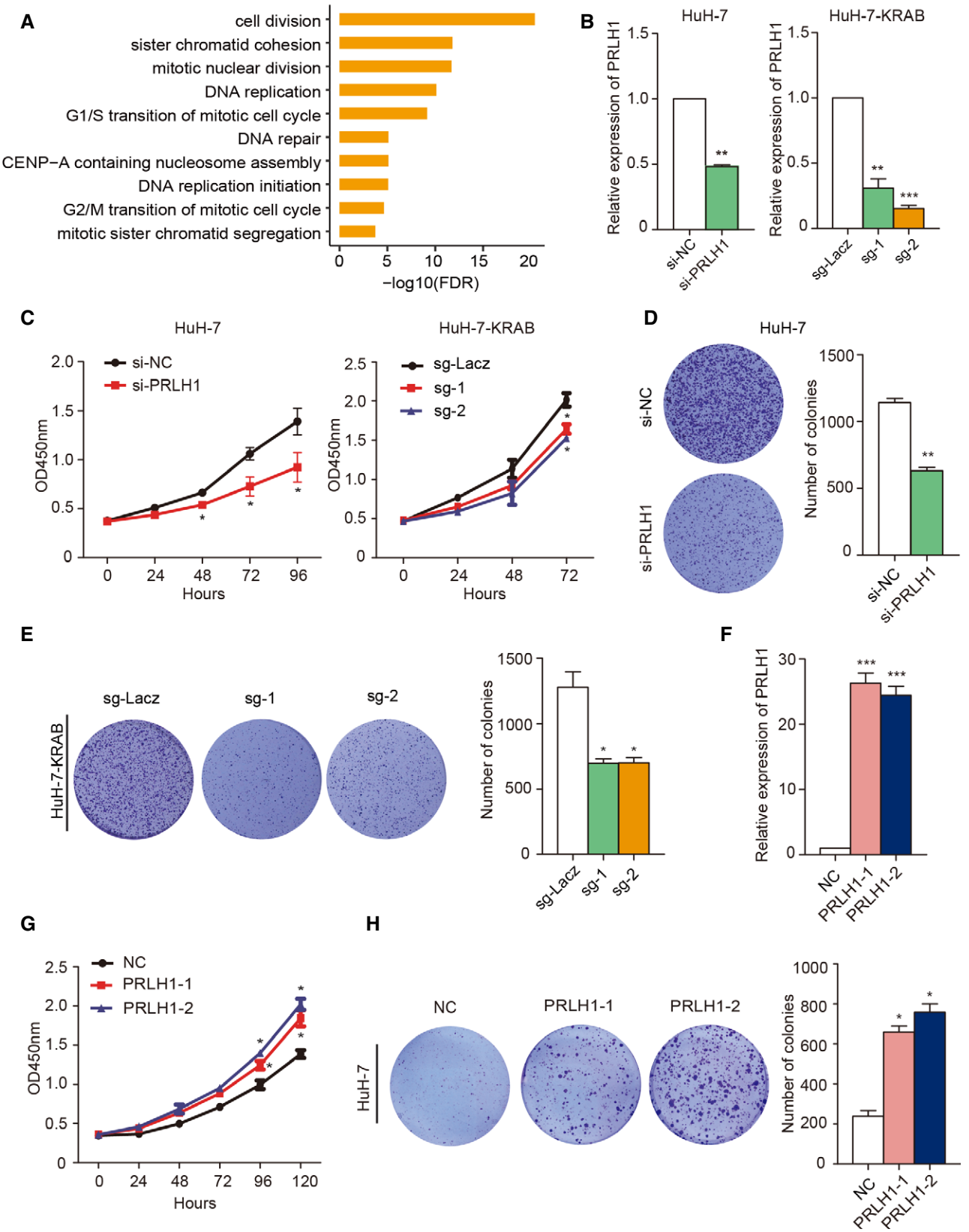

Figure 3.

To identify the specific PRLH1 transcript segment that was responsible for the RNF169 binding, we truncated PRLH1 in different regions and performed RNA pull-down assays using these deletion mutants followed by the Western blot. As RNF169 protein is mainly located in the nucleus, we resolved the nuclear proteins of HuH-7 cells to incubate with the full-length or truncated PRLH1 RNAs in RNA pull-down assays. The result showed that a 215-nt region (nts 114–328) in the 5′ exon of the PRLH1 transcript was necessary for the binding of PRLH1 to RNF169 (Fig 4F). To identify the sequence motif bound by RNF169 on PRLH1 RNA, we screened the sequence of the 215-nt region (nts 114–328) and found that there were two GCUUCA boxes in this region, which were conserved in 91% (2,487 of 2,742) of LTR12C copies (Table EV2). We mutated these two GCUUCA boxes and found that the binding of RNF169 significantly diminished (Fig 4G), indicating that the two GCUUCA boxes in the

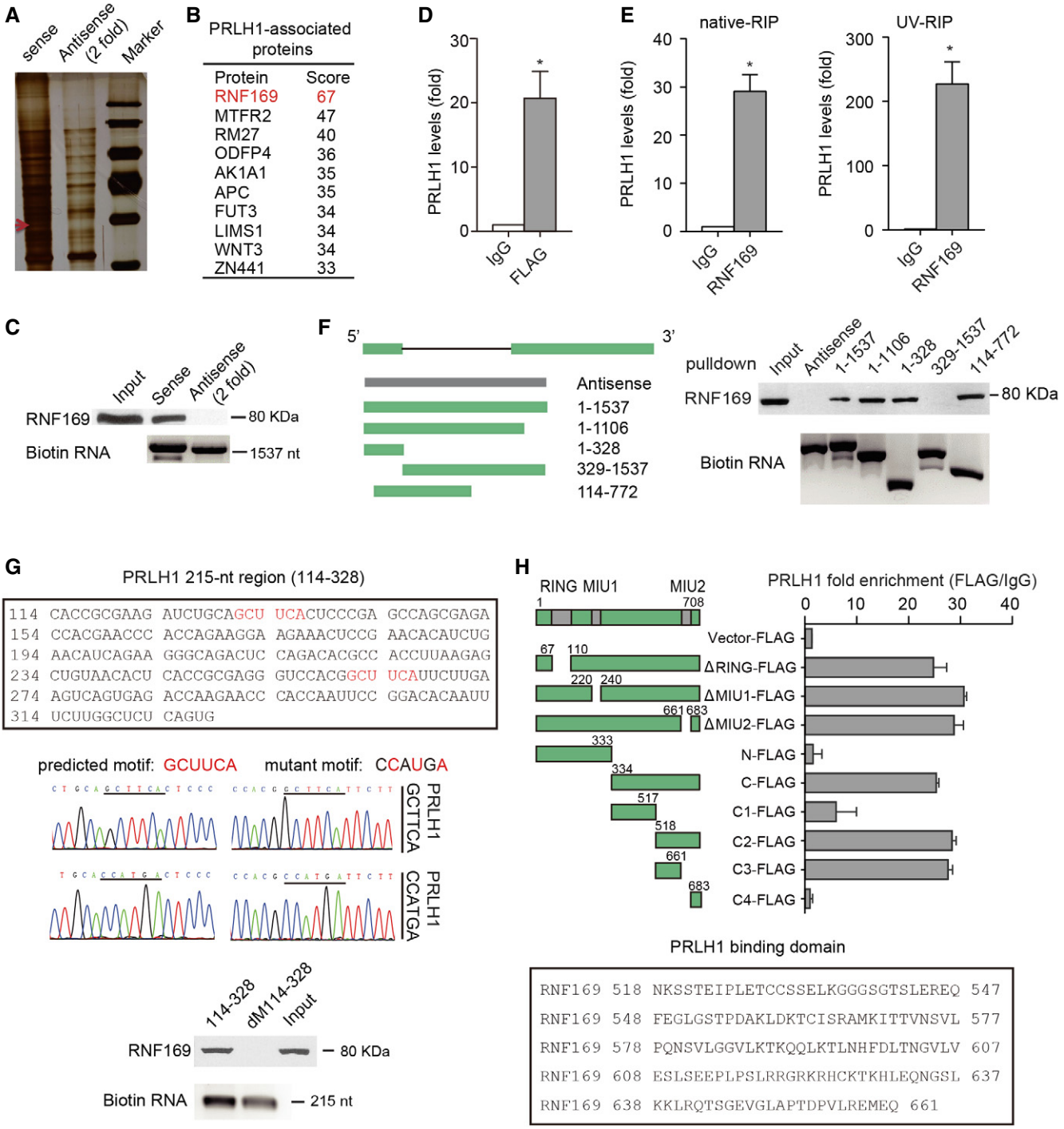

Figure 4.

Figure 4. PRLH1 specifically binds to the RNF169 protein.

A Silver staining after SDS–PAGE using the precipitates pulled down by PRLH1 and its antisense RNA from the total HuH-7 cell extracts. The band specific for PRLH1 is marked by red arrow.

B The result of MS analysis showing PRLH1-interacting proteins. RNF169 is the only protein with significance and highlighted with red font. Protein scores > 56 are significant ($P < 0.05$).

C Western blot analysis of RNF169 using the precipitates as in (A). Total extract of the HuH-7 cells was used as the input. Twofold amount of PRLH1 antisense RNA was used as a negative control.

D The PRLH1 fold enrichment in native RIP assays with the FLAG antibody using extracts from HuH-7 cells overexpressing pcDNA3.1-FLAG-RNF169. IgG was used as a negative control antibody. Error bars, SEM ($n = 3$ independent cell cultures). *$P < 0.05$ (two-tailed paired Student's *t*-test).

E The PRLH1 fold enrichment in native RIP assays and UV-crosslinking RIP assays with the RNF169 antibody in HuH-7 cells. IgG was used as a negative control antibody. Error bars, SEM ($n = 3$ independent cell cultures). *$P < 0.05$ (two-tailed paired Student's *t*-test).

F Western blot analysis of RNF169 using the precipitates pulled down by two full-length transcripts or four truncated RNA fragments of PRLH1. The diagram of truncated PRLH1 fragments is shown on the left. PRLH1 antisense RNA was used as a negative control.

G The mutation of both GCUUCA boxes on PRLH1 RNA and the binding of RNF169 to the motifs. Top, the RNA sequence of the 215-nt region (nts 114–328) of PRLH1; middle, the sequence and sequencing map of the predicted and mutant motifs; bottom, Western blot against RNF169 after RNA pull-down assays using the biotin-labeled wild-type and mutant 215-nt regions of PRLH1 RNA (114–328 and dM114–328).

H Schematic illustration of different deletion mutants of RNF169 (left) and the PRLH1 fold enrichment in RIP assays using the FLAG antibody on extracts from HuH-7 cells transfected with indicated vectors (right). The values represent mean ± SEM from two independent experiments. The amino acid sequence of PRLH1-binding domain on RNF169 is shown below.

Source data are available online for this figure.

5′ exon of PRLH1 were essential for the binding of the RNF169 protein.

We also examined whether PRLH1 bound to a specific region of the RNF169 protein. Thus, we generated a series of RNF169 deletion mutants and analyzed their ability to interact with PRLH1 by RIP assays for precise mapping of the RNA-binding domain of RNF169 polypeptide. Accordingly, the RIP results showed that the binding of RNF169 to PRLH1 did not depend on any of the three known domains of the RNF169 protein (RING, MIU1, MIU2), but the C3 region of RNF169 protein, an uncharacterized domain composed of amino acids 518–661, was essential for the binding (Fig 4H). All these results showed that RNF169 is a novel RNA-binding protein that specifically binds to two GCUUCA boxes of the PRLH1 transcript through the C-terminal and suggested that the function of PRLH1 was related to HR-mediated DNA repair.

PRLH1 promotes the HR-mediated DNA repair by limiting 53BP1 association with DSB sites

Since the E3 ubiquitin ligase RNF169 functions in the DNA damage response (DDR) and HR pathway [11,13], we investigated whether PRLH1 plays an important role in HR-mediated DNA repair with RNF169. Therefore, we first activated the DNA damage response using the anticancer drug adriamycin (ADR) in SK-HEP-1 and HuH-7 cells. The expression of PRLH1 and RNF169 was examined after treatment with different adriamycin concentrations for 48 h. As shown by qRT–PCR analysis, the relative expression levels of both PRLH1 and RNF169 were rapidly increased in a dose-dependent manner upon ADR treatment, indicating that both PRLH1 and RNF169 were involved in the DNA damage response (Fig 5A).

Next, we employed an I-SceI-dependent DR-GFP reporter assay to determine the HR repair efficiency upon PRLH1 overexpression in HuH-7 cells. The DR-GFP cells contain two GFP mutants, one of which has two premature stop codons along with one internal I-SceI endonuclease restriction site (SceGFP), and the other is 3′ and 5′ termini truncated (iGFP), neither of which expresses a functional GFP protein [51]. In this assay, homologous recombination between GFP mutants restores SceGFP to wild-type GFP, and the quantity of GFP can be examined by FACS, thereby indicating HR efficiency (Fig 5B). The FACS results showed that HR activity significantly increased after overexpression of PRLH1 or RNF169 in HuH-7-DR-GFP cells compared with the activity in cells transfected with the corresponding empty vectors (Fig 5C). Furthermore, the cell cycle distribution was not affected by the PRLH1 overexpression in HuH-7-DR-GFP cells, excluding indirect cell cycle-related effects on HR repair (Fig EV4A). Knockdown of PRLH1 could also impair HR efficiency in HuH-7-DR-GFP or HuH-7-KRAB-DR-GFP cells (Figs 5D and EV4B). These results suggest that PRLH1, as well as RNF169, is involved in the DNA damage response and promotes HR activity *in vitro*.

Given that RNF169 promotes HR activity by competing with 53BP1 for binding to the DSB sites [11,13], PRLH1 might be expected to participate in this critical process along with RNF169. To test this speculation, we assessed the effect of PRLH1 knockdown or overexpression on the subcellular distribution of 53BP1 upon exposure to ADR. As presented in Figs 5E and EV4C and D, upon ADR treatment, the number and density of 53BP1-positive foci were obviously increased in PRLH1-knockdown HuH-7 cells but diminished and attenuated in HuH-7 cells overexpressing PRLH1-1/2 or FLAG-RNF169 compared with those in the corresponding control. Together, these results clearly showed that PRLH1 plays a role similar to the RNF169 protein in antagonizing the recruitment of 53BP1 to the DSB sites in response to DNA damage, supporting the notion that the PRLH1-RNF169 complex functions at the initiation stage of HR repair.

PRLH1 stabilizes the RNF169 protein to form a functional complex in HR repair

To further explore the mechanism underlying the possible synergy between PRLH1 and RNF169, we performed an analysis of PRLH1 knockdown or overexpression to show the influence on the protein levels of RNF169 and 53BP1 in HuH-7 cells. Remarkably, the protein level of RNF169 dramatically decreased after knockdown of PRLH1 by CRISPRi or RNAi methods and increased after overexpression of PRLH1 with or without ADR treatment, while the 53BP1 protein

level exhibited nearly no change (Figs 6A and EV5A). Moreover, the mRNA level of RNF169 was not affected by PRLH1 knockdown or overexpression (Fig EV5B and C). By contrast, the overexpression of FLAG-RNF169 had no effect on PRLH1 expression (Fig EV5D). After cycloheximide (CHX) treatment for 4 or 8 h, the RNF169 protein was more rapidly degraded in PRLH1-knockdown cells than the control cells (Fig EV5E), indicating a critical role of PRLH1 for stabilizing RNF169 at the post-translational level. Importantly, PRLH1 could also control the RNF169 recruitment and retention at DSB sites (Fig 6B and C).

Next, we performed rescue assays to detect the importance of RNF169 for the functions of PRLH1. Knockdown of RNF169 in HuH-7 cells could rescue the reduced 53BP1 foci, enhanced RAD51 recruitment, and decreased HR efficiency caused by the

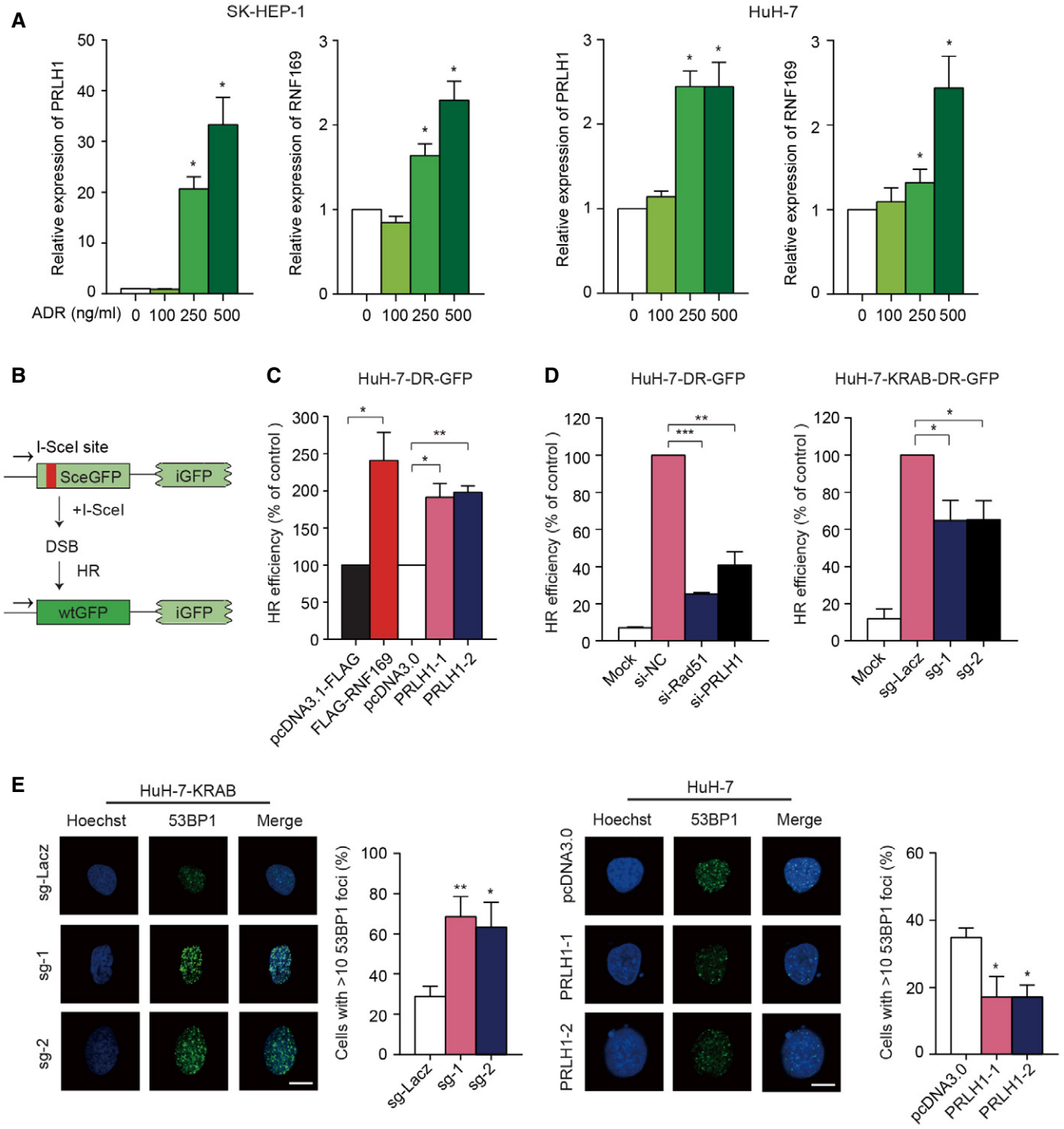

Figure 5.

Figure 5. PRLH1 promotes the HR activity by antagonizing the recruitment of 53BP1.

A The relative expression of PRLH1 and RNF169 in SK-HEP-1 and HuH-7 cells treated with ADR for 48 h.

B Schematic of the HR reporter system. SceGFP, the mutant GFP with two premature stop codons and one internal I-SceI endonuclease restriction site; iGFP, the mutant GFP with the 3′ and 5′ termini truncated; wtGFP, wild-type GFP.

C HR activity in HuH-7-DR-GFP cells overexpressing PRLH1 or RNF169. The HuH-7-DR-GFP cells were transfected with the PRLH1 or RNF169 vectors for 24 h before transfection with the I-SceI plasmid for another 48 h. The HR efficiency is shown as % of control. The values in the pcDNA3.0- or pcDNA3.1-FLAG-transfected group were used as control for normalization

D HR activity in HuH-7-DR-GFP or HuH-7-KRAB-DR-GFP cells after knockdown of PRLH1. The cells were transfected with the indicated siRNAs or sgRNA plasmids for 24 h before transfection with the I-SceI plasmid for another 48 h. The values in the si-NC- or sg-Lacz-transfected group were used as control for normalization. The Mock group without transient transfection of siRNAs, sgRNA, or I-SceI plasmids in the corresponding cells was used as a negative control.

E The recruitment of 53BP1 to DSB sites after knockdown or overexpression of PRLH1 with 500 ng/ml ADR treatment for 24 h. Left, representative pictures and quantification of cells with 53BP1-positive foci in HuH-7-KRAB cells transfected with two sgRNAs for PRLH1 (sg-1, sg-2) or a control sgRNA (sg-Lacz). Right, representative pictures and quantification of cells with 53BP1-positive foci in HuH-7 cells transfected with pcDNA3.0-PRLH1-1/2 or control vector. Scale bars, 10 μm.

Data information: In (A, C–E), error bars, SEM (n = 3 independent cell cultures). *P < 0.05; **P < 0.01; and ***P < 0.001 by two-tailed paired Student's t-test.

PRLH1 overexpression (Figs 6D and E, and EV5F). We found that overexpression of RNF169 could significantly promote cell proliferation in HuH-7 cells (Fig EV5G). The increased cell growth ability in PRLH1-overexpressing HuH-7 cells could also be reverted by knockdown of RNF169 (Fig 6F and G). All these results suggest that the interplay between PRLH1 and RNF169 may be beneficial for the formation of a more stable complex to promote the initiation of HR repair.

Discussion

Previous studies have shown that the HR machinery is made up of various protein factors [4,10]. Although several lncRNAs may be involved in the regulation of the HR processes [28–30], few are characterized as HR components. In this study, we first identified a RNF169-interacting lncRNA PRLH1 that promoted HR repair. In our model, PRLH1, which is activated by NF-Y and repressed by p53, specifically binds to the C terminus of RNF169 to form a stable RNA–protein complex. This complex can compete with and displace 53BP1 from the ubiquitin-modified DSB sites, thus promoting the initiation of HR repair (Fig 7). Since the RNF169 protein was reported to form a high-affinity complex at the DSB sites, in contrast to 53BP1 [13], we propose that PRLH1 might contribute and be required for the high affinity of RNF169 by forming a stable RNA–protein complex, such as a DNA repairosome. Panier *et al* reported that the RNF169 protein accumulated at DSB sites through the use of specific peptide motifs named LRMs [52]. Therefore, our study indicated that the accumulation of RNF169 at DSB sites might not only depend on its peptide motifs but also depend on its binding lncRNA PRLH1.

p53 acts as a major tumor suppressor by regulating the cell cycle, apoptosis, and DNA repair in cells [14,53,54]. Distinctly, p53 inhibits HR repair to maintain genome integrity by directly interacting with several key HR protein factors, such as RAD51 and RAD54, and interfering with their functions [24,25]. Therefore, the suppression of HR by p53 has been considered largely independent of its transactivation function [20,55,56], although p53 can also downregulate RAD51 transcription [27]. In our study, we also confirmed that knockdown of wild-type p53 could significantly increase HR efficiency (Appendix Fig S3A). Furthermore, we identified a new p53/PRLH1 pathway to repress HR repair, demonstrating a transcription-dependent regulation of HR repair by p53. Our results, therefore, indicate that the transcriptional control by p53 and NF-Y is essential not only for cell cycle regulatory genes [16,43,46] but also for lncRNAs in HR repair. Early studies have shown that p53 could repress some cell cycle genes activated by NF-Y through the p53-p21-DREAM-CDE/CHR pathway [57,58], but no CDE/CHR motifs could be observed on the PRLH1 promoter, indicating p53 regulates the PRLH1 expression in a different way. We performed Co-IP assays in p53 wild-type and mutated HCC cells, but no interaction between p53 and NF-YB was observed in our results (Appendix Fig

Figure 6. PRLH1 stabilizes the RNF169 protein at DSB sites and functions dependent on RNF169.

A The protein level of RNF169 and 53BP1 in HuH-7 cells knocked down or overexpressing PRLH1 with or without 500 ng/ml ADR treatment for 24 h. Left, HuH-7-KRAB cells were transfected with two sgRNAs for PRLH1 (sg-1, sg-2) or a control sgRNA (sg-Lacz) for 24 h before ADR treatment. Right, HuH-7 cells were transfected with pcDNA3.0-PRLH1-1/2, pcDNA3.1-FLAG-RNF169, or the control vectors for 24 h before ADR treatment. Numbers represent the relative intensities of Western blot bands of 53BP1 or RNF169, normalized to GAPDH.

B The recruitment of RNF169 to DSB sites after knockdown or overexpression of PRLH1 with 500 ng/ml ADR treatment for 24 h. Representative pictures of cells with RNF169-positive foci in HuH-7 and HuH-7-KRAB cells transfected with the indicated plasmids or siRNAs were shown. Scale bars, 10 μm.

C Quantification of cells with RNF169-positive foci in (B). Error bars, SEM (n = 3 independent cell cultures). *P < 0.05; **P < 0.01; and ***P < 0.001 by two-tailed paired Student's t-test.

D Representative pictures and quantification of cells with 53BP1 and RAD51 foci in HuH-7 cells co-transfected with the indicated plasmids and siRNAs. Error bars, SEM (n = 3 independent cell cultures). **P < 0.01 and ***P < 0.001 by two-tailed paired Student's t-test. NS means no significance.

E HR efficiency in HuH-7 cells co-transfected with the indicated plasmids and siRNAs. Error bars, SEM (n = 3 independent cell cultures). **P < 0.01 and ***P < 0.001 by two-tailed paired Student's t-test. NS means no significance.

F, G CCK-8 assays (F) and colony formation assays (G) showing the cell viability in HuH-7 cells co-transfected with the indicated plasmids and siRNAs. Error bars, SEM (n = 3 independent cell cultures). *P < 0.05 by two-tailed paired Student's t-test. NS means no significance.

Source data are available online for this figure.

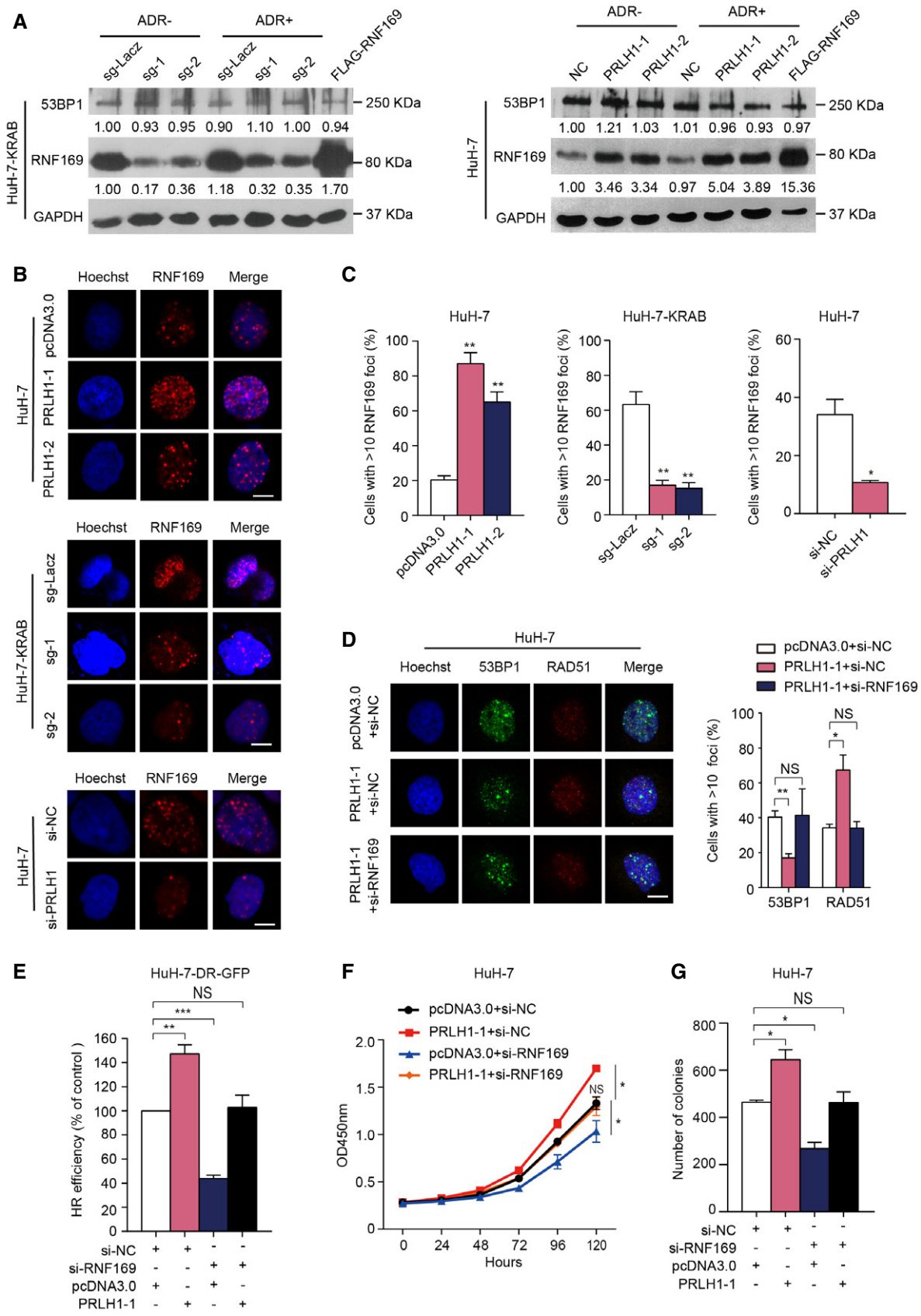
A
ADR-
ADR+
sg-Lacz
sg-1
sg-2
FLAG-RNF169
HuH-7-KRAB
53BP1
RNF169
GAPDH
250 KDa
80 KDa
37 KDa
1.00 0.93 0.95 0.90 1.10 1.00 0.94
1.00 0.17 0.36 1.18 0.32 0.35 1.70
NC
PRLH1-1
PRLH1-2
HuH-7
1.00 1.21 1.03 1.01 0.96 0.93 0.97
1.00 3.46 3.34 0.97 5.04 3.89 15.36
B
Hoechst
RNF169
Merge
pcDNA3.0
PRLH1-1
PRLH1-2
sg-Lacz
sg-1
sg-2
si-NC
si-PRLH1
C
HuH-7
HuH-7-KRAB
Cells with >10 RNF169 foci (%)
si-NC
si-PRLH1
D
53BP1
RAD51
pcDNA3.0+si-NC
PRLH1-1+si-NC
PRLH1-1+si-RNF169
NS
E
HuH-7-DR-GFP
HR efficiency (% of control)
si-RNF169
pcDNA3.0
PRLH1-1
F
OD450nm
Hours
G
Number of colonies

Figure 6.

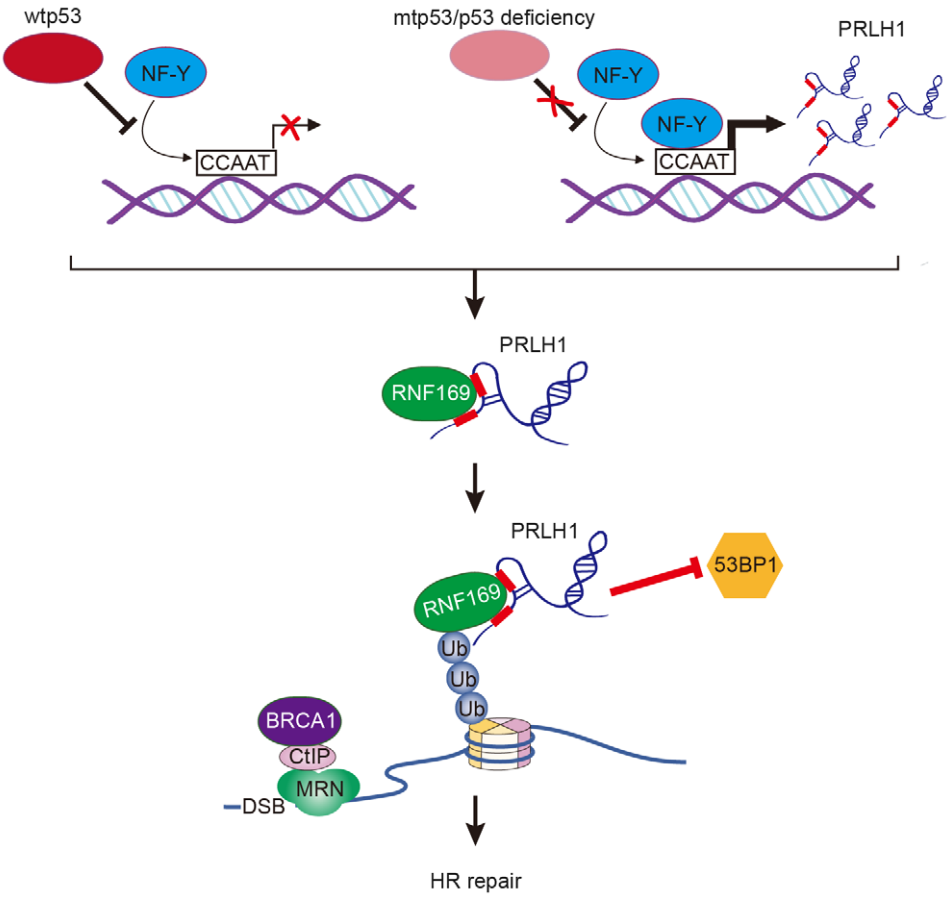

Figure 7. The proposed model for the transcriptional regulation and function of PRLH1.

In wild-type p53 (wtp53) cells, the binding of NF-Y to the PRLH1 promoter is inhibited by p53, and thus, the transcription of PRLH1 is repressed, while in mutant p53 (mtp53) or p53-deficient cells, mtp53 or p53 deficiency fails to inhibit the binding of NF-Y to the promoter of PRLH1, leading to the high expression of PRLH1 in these cells. PRLH1 can specifically bind to the RNF169 protein through two GCUUCA motifs, which are represented by two red boxes in the PRLH1 transcript. Subsequently, the PRLH1-RNF169 complex displaces 53BP1 from the ubiquitin-modified chromatin at DSB sites. The MRN-CtIP-BRCA1 complex then accumulates in DSB sites to allow extensive DSB resection, thereby leading to an increase in HR activity.

S3B). The ChIP assays also showed that p53 could not bind to the CCAAT motifs on the PRLH1 promoter in these cells (Appendix Fig S3C). Thus, we suppose that p53 prevents the binding of NF-Y to the PRLH1 promoter in an indirect way rather than directly interacting with NF-Y. The ERV-9 LTR retrotransposon was reported to be hypermethylated, and TF-binding sites on it overlapped by CpGs displayed reduced affinities for the responding TFs [59]. Since p53 could constrain the retrotransposons by epigenetic regulation, such as regulating the CpG methylation [60], and interact with DNMT1 and DNMT3a to execute p53-mediated gene repression [61,62], it was possible that p53 might inhibit the binding of NF-Y to the PRLH1 promoter by promoting the CpG methylation of its promoter.

As reported, cells harboring p53 hot spot mutants often have high HR activity to overcome serious DNA damage [23,63], and exacerbated HR activity contributes to genome instability and tumorigenesis [21–23]. In our study, PRLH1 is highly expressed in p53-mutated HCC samples and cells, indicating that PRLH1 may be a key effector for enhanced HR activity and genome instability in the p53-mutated HuH-7 cells. Intriguingly, exogenous expression of PRLH1 promoted cell proliferation in the p53-mutated cell line HuH-7 but not in two p53 wild-type cell lines, HepG2 and SK-HEP-1. Meanwhile, even though PRLH1 promoted HR repair in HuH-7 cells, no significant effect was observed on HR efficiency in the p53 wild-type HCC cell line HepG2 after overexpression of PRLH1 (Appendix Fig S3D). We speculate that overexpression of PRLH1 may contribute to exacerbated HR activity in HuH-7 cells with high HR activity so that its carcinogenesis leads to the promotion of cell proliferation, while overexpression of PRLH1 in two p53 wild-type HCC cells (SK-HEP-1 and HepG2) with low HR activity could not lead to significant promotion of HR repair maybe because of the repression by p53 on HR repair and the lack of other HR factors, and thus fail to increase growth in these cells. Furthermore, the expression of PRLH1 and RNF169 was markedly increased in HCC cells in our DDR assays; thus, hepatocellular carcinoma cells may promptly activate the HR pathway for survival under conditions of serious stress, such as DNA damage.

The ERV-9 lncRNAs are a big RNA family transcribed from many of ~4,000 copies of the ERV-9 LTR retrotransposons across the

human genome [37,38,64], among which 2,742 copies belong to the LTR12C subfamily. PRLH1 and its lncRNA counterparts were identified in this study as members of the ERV-9 RNA family since they were all derived from LTR12C elements. The 5′-terminal region of PRLH1, especially two GCUUCA boxes, which are essential for the binding to RNF169, is highly conserved in these LTR12C copies (Table EV2). The ERV-9 LTRs are conserved during primate evolution [65] and usually bound by NF-Y transcriptional factor [37,38], implying that their transcription and regulation may be under control of the p53 pathway. So far, however, the biological significance of this transcriptional control has not been well understood due to the unclear function of retrotransposon-derived RNAs. In contrast to the parasitic transcripts, ERV-9 lncRNAs have been reported to act in cis to facilitate the long-range LTR enhancer function in activating transcription of downstream, cis-linked globin genes in human erythroblasts [37]. In this study, we found a previously unknown function of the ERV-9 lncRNA PRLH1 in the HR repair and the mechanism underlying the inhibition of HR through transcriptional suppression of LTR retrotransposons by the p53/NF-Y pathway. Interestingly, we found that PRLH1 and another 17 LTR12C-derived lncRNAs were specifically expressed in human testis according to the GTEx RNA-seq data analysis (Appendix Fig S4 and Tables EV3 and EV4). These discoveries suggest that ERV-9 lncRNA family, transcribed from a large class of LTR retrotransposons which comprise ~10% of the human genome and are generally regarded as parasites or "Junk DNA" [31,32], may have a potential role in testis cells, suggesting the importance of LTR retrotransposons in the evolution of the human genome.

In summary, in this study, we characterized a p53-repressed lncRNA PRLH1 that interacts with RNF169 as a positive regulator of HR activity. Our study reveals a novel RNA–protein interplay involved in HR and sheds light on the function and regulation of the LTR retrotransposon-derived lncRNA family.

Materials and Methods

RNA-seq data processing and differential expression analyses

Raw RNA-sequencing reads and the corresponding clinical information of 371 primary tumors and 50 normal samples for HCC were downloaded at the TCGA Data Portal (Data ref: GDC Data Portal TCGA-LIHC, 2015) [66]. The reads were processed and normalized using the Rsubread package [67,68] (version 1.14.2) and aligned to the UCSC hg19 reference genome. The feature Counts function was used to summarize the gene expression values as integers. These summarized gene values were then normalized to FPKM values. lncRNAs annotated by GENCODE version 19 were used in present study. We filtered out the lncRNAs overlapping the protein-coding genes using BEDTools [69] and obtained a more accurate lncRNA annotation set. The p53 mutation data of tumor samples were obtained from cBioPortal [70]. Significant differences in the expression of lncRNAs between two groups were estimated using the voom [71] function of the "limma" package in R.

GO enrichment analysis

We first detected the protein-coding genes with significantly differential expression between HCC tumor and normal tissues and chose genes with fold-changes ≥ 2 and FDR < 0.05. The FPKM values were log2-transformed, and Pearson's correlation coefficient was used to estimate the relationship of PRLH1 and each differentially expressed protein-coding gene. The *P*-values of the correlation coefficient for each pair were calculated using Fisher's asymptotic test. The correlated protein-coding genes with $|r| > 0.2$ and $P < 0.05$ were submitted to DAVID [72] for GO enrichment analysis.

Cell culture, RNAi, and transfection

The HepG2 and PLC/PRF/5 cell lines were cultured in MEM (Gibco) supplemented with 10% fetal bovine serum (Gibco). The SMMC-7721 cell line was cultured in RPMI 1640 medium (Gibco) supplemented with 10% fetal bovine serum (Gibco). The 293T, LO2, HuH-7, and SK-HEP-1 cells were cultured in DMEM (Gibco) supplemented with 10% fetal bovine serum (Gibco). Cells were cultured at 37°C in the 5% CO_2. For DNA damage, cells were treated with 500 ng/ml doxorubicin hydrochloride (Sigma, D1515). siRNA transfection was performed at a final concentration of 50 nM using Lipofectamine 2000 (Invitrogen) according to the manufacturer's instruction. Transfection of plasmids was performed using ViaFect Reagent (Promega). All siRNAs used in this study were purchased from GenPharma, and the sequences of the siRNAs are listed in Table EV5.

Rapid amplification of cDNA ends (5′- and 3′-RACE)

One microgram of HuH-7 total RNA was purified by treating with recombinant DNase I (RNase-free, TaKaRa), and then, RACE assays were performed using the 5′-Full RACE and 3′-Full RACE kits (TaKaRa) according to the manufacturer's instructions. Specific 5′- and 3′-RACE cDNA fragments were acquired using the universal primer mix provided by the kit, and then, gene-specific primers (GSPs) were used for the nested PCR. The PCR products were subcloned into pMD™19-T Vector (TaKaRa) and sequenced. The GSP sequences are listed in Table EV5.

Plasmid construction

For RNF169 and PRLH1 overexpression, the CDS sequence of RNF169 or the full-length sequences of two PRLH1 transcripts were cloned into pcDNA3.1-FLAG or pcDNA3.0 plasmid, respectively. For p53 and NF-YB overexpression, the CDS sequences of wild-type p53 or NF-YB were cloned into pcDNA3.0 plasmid and pcDNA3.1 plasmid, respectively. For construction of the PRLH1-ORF-3×FLAG and hMinion-3×FLAG plasmids, three predicted ORFs with 5′-UTR sequences of lncRNA PRLH1 and the CDS of hMinion gene were cloned into the EcoRV site of the modified pCH-3×FLAG vector using the ClonExpress II One Step Cloning Kit (Vazyme), respectively. For construction of the promoter–reporter vectors, the PRLH1 promoter (-984 to +36 bp) was cloned into the pGL4.11 vector in front of the luciferase coding sequence to generate the wild-type vector. Then, the Multipoints Mutagenesis Kit (TaKaRa) was used to generate various CCAAT-mutant PRLH1 promoter vectors. For knockout of TP53 in HepG2 cells, two sgRNAs were designed based on CRISPR sgRNA Design tool (CHOPCHOP) and inserted into PX462 (a gift from Jianyou Liao, Research Center of Medicine, Sun Yat-sen Memorial Hospital, Sun Yat-sen University, Guangzhou,

China; Addgene, #62987) together to generate the PX462-KO-p53 vector. For knockdown of PRLH1 in HuH-7-KRAB cells, two sgRNAs were designed based on CHOPCHOP and inserted into pU6-sgRNA plasmid to generate two PRLH1 sgRNA vectors. For RIP assays, the sequences of deletion mutants of RNF169 were cloned into the pcDNA3.1-FLAG plasmid from the full-length CDS of RNF169 using the corresponding primers. For RNA pull-down assays, the sequences of the PRLH1-1 transcript (1–1,537), the PRLH1-2 transcript (1–1,106), the 5′ exon (1–328), the 3′ exon (329–1,537), the two-side truncated fragment (114–772), the wild-type and mutant PRLH1 215-nt region (114–328 and dM114–328), and the long full-length antisense PRLH1 were cloned between the KpnI and XhoI sites of pcDNA3.0 for *in vitro* transcription. All constructs were verified by sequencing. The primers for plasmid construction are listed in Table EV5.

Generation of the HuH-7-KRAB and HepG2-KRAB cell lines

The HuH-7-KRAB and HepG2-KRAB stable cell lines were generated using the CRISPRi system. Lenti-dCas9-KRAB plasmid was co-transfected with the second-generation packaging plasmid psPAX2 (Addgene plasmid #12260) and the envelope plasmid pMD2.G (Addgene plasmid #12259) into 293T cells for 2 days, and supernatants containing lentivirus were collected and concentrated. The HuH-7 and HepG2 cells were infected with the packaged lenti-dCas9-KRAB plasmid and selected with blasticidin (10 μg/ml) for a week. Then, the stable HuH-7-KRAB and HepG2-KRAB cell lines were obtained and cultured with 5 μg/ml blasticidin.

Knockout of TP53

The CRISPR/Cas9 nickase system was used to generate the HepG2-KO-p53 cell line. The HepG2 cells were transfected with PX462-KO-p53 plasmid and cultured in the presence of puromycin (2 μg/ml) for 48 h after transfection. Single-cell clones were generated by limited-dilution assays and tested for knockout of TP53 protein by Western blot. The primers for T7E1 assay and detection of p53 gene mutation are listed in Table EV5.

RNA extraction and qRT–PCR

Total RNA was isolated using TRIzol (Invitrogen). Nine kinds of human normal tissue RNA were purchased from Clontech. cDNA was synthesized using a PrimeScript™ RT Reagent Kit with gDNA Eraser Kit (TaKaRa) according to the manufacturer's protocol. qPCRs were performed in triplicates with the SYBR® Premix Ex Taq™ II (TaKaRa) on a Step One Plus Real-Time PCR System (Applied Biosystems, CA). Normalization was performed with GAPDH. The ΔΔCt method for relative quantitation (RQ) of gene expression was used and generated using the equation $2^{-\Delta\Delta Ct}$. The primers for qRT–PCR are listed in Table EV5.

Western blot

Cells were lysed in RIPA lysis buffer supplemented with protease inhibitor cocktail (Roche) on ice for 30 min and then denatured at 99°C for 10 min. Cell lysates were separated by 10% SDS–PAGE and then transferred to a 0.2 μM nitrocellulose (NC) membrane (Millipore). Primary antibodies used were as follows: anti-histone H3 (4499S, CST), anti-GAPDH (2118S, CST), anti-RAD51 (ab88572, Abcam), anti-β-tubulin (10094-1-AP, Proteintech), anti-53BP1 (sc-22760, Santa Cruz), anti-RNF169 (ab87711, Abcam), and anti-FLAG (M20008, Abmart).

Nuclear–cytoplasmic fractionation

A total of 10^7 HuH-7 cells were collected by trypsinization, and the pellets were resuspended in 380 μl ice-cold HLB [10 mM Tris (pH 7.5), 10 mM NaCl, 3 mM $MgCl_2$, 0.3% (vol/vol) NP-40, and 10% (vol/vol) glycerol] supplemented with 1× protease inhibitor cocktail (Roche) and 40 U/μl of RRI (TaKaRa) and 1 M DTT]. The mixture was incubated on ice for 10 min and briefly vortexed,and then, the cells were centrifuged at 1,000 *g* at 4°C for 3 min. The supernatant was carefully transferred by pipette to a new tube, and the pellet was kept on ice. The supernatant contained the cytoplasmic fraction. To it, 1 ml RNA precipitation solution (RPS) was immediately added, and the sample was stored at −20°C for at least 1 h. The pellet was washed with 1 ml ice-cold HLB three times by gently pipetting up and down and then centrifuged at 200 *g* at 4°C for 2 min. Samples incubated in RPS at −20°C for > 1 h were vortexed for 30 s and then centrifuged at 18,000 *g* at 4°C for 15 min. The supernatant was discarded, and the pellet was washed by vortexing in ice-cold 75% (vol/vol) ethanol and centrifuged at 18,000 *g* at 4°C for 5 min. The supernatant was discarded, and the pellet was partially air-dried. One ml of TRIzol was added to semidry pellets. To all samples in TRIzol, 10 μl of 0.5 M EDTA was added and samples were heated to 65°C with vortexing until the pellet was dissolved (~10 min). The RNA and protein were then extracted from nuclear and cytoplasmic fractions using TRIzol. The primers used to detect the distribution are listed in Table EV5.

Cell counting Kit-8 (CCK-8) assays

For CCK-8 assays, cells were seeded at a concentration of 2,500–5,000 cells/well in 96-well plates after transfection with siRNAs at 50 nM or with 1 μg pcDNA3.0-PRLH1-1/2 in 12-well plates for 24 h. Cell numbers were quantified using CCK-8 reagent (Cat# CK04, DOJinDO) at the indicated time according to the manufacturer's instructions.

Colony formation assays

For colony formation assays, 1×10^4 cells were seeded into 60-mm dishes after transfection with siRNA or plasmid for 24 h. Colonies, which were allowed to form for 12 days after plating, were stained with a crystal violet solution and counted. Assays were done in triplicate.

Luciferase assays

For luciferase assays, 1.5×10^4 HuH-7 cells or 1.2×10^4 SK-HEP-1 cells were seeded into 96-well plates. After 24 h, the pGL4.11 promoter–reporter vectors were transfected into the indicated cells for luciferase activity. After 48 h of incubation, the cells were lysed using the passive lysis buffer and the luciferase activity was detected using the dual-luciferase assay system (Promega).

Chromatin immunoprecipitation (ChIP)

ChIP assays were performed as previously described [73]. HuH-7, SK-HEP-1, or HepG2 cells (5×10^6) with or without 500 ng/ml ADR treatment for 24 h were harvested for ChIP assays. Cells were cross-linked with 1% formaldehyde at room temperature for 10 min and then neutralized with 125 mM glycine for 5 min. Cells were rinsed with ice-cold PBS twice and scraped into ice-cold PBS. The cells were lysed in cell lysis buffer and then in nuclear lysis buffer. After sonication, supernatants were collected and diluted in ChIP dilution buffer and pre-cleared with 60 μl of Protein G Magnetic Beads (Invitrogen). Ten microliter (1%) of the supernatant was reserved as an input sample. Cleared samples were incubated with 2 μg anti-NF-YB (sc-376546, Santa Cruz) or anti-p53 (2524S, CST) antibody or normal mouse IgG (12-371, Millipore) overnight at 4°C. After immunoprecipitation, 50 μl Protein G Magnetic Beads were added and incubated for another 2 h at 4°C. Then, the precipitates were washed, and DNA was purified using Qiagen PCR purification kit after removal of crosslinks for real-time PCR. Primers are listed in Table EV5.

RNA pull-down assay

PRLH1 and the antisense of PRLH1 fragments were amplified with primers containing T7 promoter sequences (Table EV5) and used as templates for the TranscriptAid T7 High Yield Transcription Kit (Thermo Fisher Scientific). *In vitro*-transcribed RNA was treated with DNase I and purified with the GeneJET RNA Purification Kit (Thermo Fisher Scientific). Then, 50 pmol purified biotinylated RNA was heated to 90°C for 2 min, then slowly cooled to 4°C. HuH-7 cells (2×10^7) were harvested by scraping and snap-freezing before resuspension in 200 μl lysis buffer [150 mM KCl, 25 mM Tris (pH 7.4), 0.5 mM DTT, 0.5% NP-40, 1 mM PMSF, 1× protease inhibitor cocktail (Roche), and 100 U/ml of SUPERaseIN (Ambion)] and then put on ice for 30 min. Lysates were sonicated using a VibraCell Sonicator VCX130PB for 10 min with 10 s-on/30 s-off cycles. After that, the supernatants of lysates were incubated with Pierce Magnetic RNA-Protein Pull-Down Kit (Thermo Fisher Scientific) according to the manufacturer's protocol. Then, the eluted proteins were detected by Western blotting or MS analysis. Antibodies used for Western blotting were anti-RNF169 (Ab87711, Abcam).

Native RNA immunoprecipitation (RIP)

For native RIP, 1×10^7 cells HuH-7 cells were resuspended in 1 ml polysome lysis buffer [PLB; 10 mM HEPES (pH 7.0), 100 mM KCl, 5 mM $MgCl_2$, 0.5% NP-40, 1 mM DTT, 100 U/ml RRI, 400 μM RVC, 1 mM PMSF, 1 × Roche protease inhibitor cocktail] and incubated on ice for 30 min. The lysates were incubated with 5 μg of FLAG antibody (M20008, Abmart), RNF169 antibody (LS-C290741-100, Lifespan) or normal mouse IgG (12-371, Millipore) overnight at 4°C, followed by lysate incubation with 100 μl prewashed Protein G Magnetic Beads (Invitrogen) for 4 h at 4°C. Then, the beads were washed four times with NT2 buffer (50 mM Tris–HCl (pH 7.4), 1 mM $MgCl_2$, 150 mM NaCl, 0.05% NP-40). Ten percent of the beads were resuspended in 1× SDS–PAGE loading buffer for Western blotting, and RNA was isolated from the remaining beads using TRIzol. Primers for qRT–PCR are listed in Table EV5.

UV-RNA immunoprecipitation

The ultraviolet-crosslinking RNA immunoprecipitation (UV-RIP) experiments were performed following standard protocols [74]. Briefly, 1×10^7 HuH-7 cells were UV-crosslinked at 254 nm (2,000 J/m^2) in 10 ml ice-cold PBS and collected by cell scraper. The cell pellets were incubated in lysis buffer (50 mM Tris–HCl (pH 7.4), 1% NP-40, 0.5% sodium deoxycholate, 100 mM NaCl, 400 U/ml RNase Inhibitor (Thermo Fisher Scientific), and protease inhibitor cocktail (Roche)) at 4°C for 20 min with rotation, followed by DNase I treatment (40 U/ml of Promega DNase I, 5 min at 37°C). After centrifugation, the supernatant was pre-cleared with 10 μl Dynabeads® Protein G at 4°C for 1 h with rotation, and then, the pre-cleared lysate was incubated with 3 μg of IgG or RNF169 antibodies overnight at 4°C. The next day, the protein–antibodies complex was incubated with Dynabeads® Protein G for 3 h at 4°C. Subsequently, beads were washed twice with cooled high-salt wash buffer and washed another twice with cooled low-salt wash buffer. Then, the beads were incubated with 100 μl low-salt wash buffer containing 100 μg of Proteinase K (Roche) for 30 min at 55°C. RNA was extracted by phenol–chloroform extraction followed by ethanol precipitation.

tRSA RNA pull-down assay

PRLH1 full-length or PRLH1-2 sequence was cloned into pcDNA3.1 plasmid with the tRSA tag at its 5′ end. The corresponding RNA products were *in vitro*-transcribed using the TranscriptAid T7 High Yield Transcription Kit (Thermo Fisher Scientific). tRSA RNA pull-down assays were performed according to previous report [75] with some modifications. Briefly, HuH-7 cells were harvested and resuspended in 1 ml of lysis buffer (10 mM HEPES (pH 7.0), 200 mM NaCl, 1 mM DTT, 1% Triton X-100, and 1 × protease inhibitor cocktail (Roche)), followed by sonication for 6 × 30 s on, with an interval of 30 s off at 4°C using the Bioruptor. And then, the ultrasonic product was centrifuged at 15,871 *g* for 10 min at 4°C. After centrifugation, the supernatant was pre-cleared with 50 μl streptavidin Dynabeads (NEB, M1420) for 20 min at 4°C, followed by the addition of 20 mg/ml yeast tRNA for 20 min at 4°C. The folded RNAs were added to the pre-cleared lysate supernatant and incubated for 4 h at 4°C, followed by washing 4 × 5 min with wash buffer (10 mM HEPES (pH 7.0), 400 mM NaCl, 1 mM DTT, 1% Triton X-100, protease inhibitor cocktail (Roche), and 2 mM RVC). The protein complex was eluted from beads by adding 50 μl of 1× SDS loading buffer and boiling for 10 min at 99°C. Eluted proteins were analyzed by WB with primary antibodies anti-RNF169 (Ab87711, Abcam) and anti-RNF168 (21393-1-AP, Proteintech).

Homologous recombination assays

HuH-7, HuH-7-KRAB, SK-HEP-1, HepG2, or HepG2-KO-p53 cells were transfected with pDRGFP for 24 h, and cells with the integrated plasmids were selected with medium containing 1.0 μg/ml puromycin. The DR-GFP cells were cultured to expand for subsequent experiments. HR assays were performed upon overexpression or knockdown of PRLH1 or RNF169 before transfection with pCBASceI to induce a double-strand break at the I-SceI site of SceGFP in DR-GFP cells. HR efficiencies were analyzed by FACS and shown as % GFP cells. Plasmids pCBASceI (Addgene plasmid

#26477) and pDRGFP (Addgene plasmid # 26475) were obtained from Maria Jasin via Addgene repository [51,76].

Cell cycle analysis

The HuH-7-DR-GFP cells were transfected with the pCBASceI plasmid for another 48 h after transfection with pcDNA3.0 or pcDNA3.0-PRLH1-1 plasmid for 24 h. Then, the cells were collected and the cell cycle assays were performed using a Cell Cycle Staining Kit (MultiSciences, CCS012). Cells were labeled with propidium iodide (PI) and analyzed using a FACSCalibur flow cytometer (BD Biosciences).

Immunofluorescence microscopy

After transfection for 24 h in HuH-7 or HuH-7-KRAB cells, the cells were treated with 500 ng/ml ADR for 24 h and fixed with 4% buffered paraformaldehyde in PBS for 30 min at room temperature. Cells were subsequently permeabilized with 0.5% Triton X-100 in PBS. Then, cells were blocked in 5% BSA in 1× PBS for 1 h. Blocked cells were incubated with antibodies for 53BP1 (1:100; sc-22760, Santa Cruz), RAD51 (1:400; ab88572, Abcam), RNF169 (1:200; NBP2-58205, Novus), or FLAG (1:100; M20008, Abmart) overnight at 4°C. Cells were then washed with PBS three times and incubated with the secondary fluorophore-conjugated antibody for 1 h at room temperature. Nuclei were labeled using 10 μg/ml Hoechst 33342 for 5 min, and images were acquired on a ZEISS fluorescence microscope using a 63× objective.

Cycloheximide chase experiment

HuH-7 or HuH-7-KRAB cells were transfected with the indicated siRNAs or plasmids for 24 h, then replaced the DMEM culture medium containing 50 μg/ml cycloheximide (CHX). Cells were harvested at indicated time points and lysed with RIPA buffer, and the cell lysates were subjected to western blot experiments to analyze protein expression at indicated time points. The relative expression level was quantified by the ImageJ software.

Co-immunoprecipitation (Co-IP)

The cells were harvested and lysed in NETN buffer (20 mM Tris–HCl (pH 8.0), 100 mM NaCl, 0.5% NP-40 and 1 mM EDTA) supplemented with a protease inhibitor cocktail on ice for 15 min, followed by centrifugation at 15,000 ×*g* at 4°C for 10 min. The supernatants of the cell lysates were incubated with 2 μg of anti-NF-YB (sc-13045, Santa Cruz) and normal rabbit IgG (2729S, CST), or anti-p53 (2524S, CST) and mouse IgG1 (5415S, CST) antibodies overnight at 4°C while rotating. Subsequently, the bead suspensions were rotated with 40 μl Dynabeads® Protein G at 4°C for 2 h. The beads were subsequently washed four times with NETN buffer and finally eluted by directly boiling in 1× SDS loading buffer with β-mercaptoethanol.

Statistical analysis

The results were expressed as the mean ± SEM unless otherwise noted. We used two-tailed paired Student's *t*-test for comparisons between the two experimental groups. Statistical analyses were performed with GraphPad Prism 6. $P < 0.05$ was considered to be statistically significant.

Expanded View for this article is available online.

Acknowledgements
We thank The Cancer Genome Atlas (TCGA) project and its contributors for providing this valuable public data set. We also appreciate the help of Stephen Piccolo for analyzing the expression values of the RNA-seq data of HCC samples from TCGA. This work was supported by the National Key R&D Program (No. 2017YFA0504400) and the National Basic Research Program (2011CB811300) from the Ministry of Science and Technology of the People's Republic of China, and the National Natural Science Foundation of China (No. 31471223, 31671349, 31770879).

Author contributions
HZ, LHQ, BD, and WLX conceived the project and conception. WLX, BD, and CL performed the molecular and cellular biology experiments. ZLW, PHL, and JHY performed the computational and statistical analysis. BL and QJH provided technical assistance. BD, WLX, ZLW, JHY, LHQ, and HZ wrote the manuscript. LHQ and HZ supervised the project. All authors read and approved the final manuscript.

Conflict of interest
The authors declare that they have no conflict of interest.

References

1. Jackson SP, Bartek J (2009) The DNA-damage response in human biology and disease. *Nature* 461: 1071 – 1078
2. van Gent DC, Hoeijmakers JH, Kanaar R (2001) Chromosomal stability and the DNA double-stranded break connection. *Nat Rev Genet* 2: 196 – 206
3. Lieber MR, Ma Y, Pannicke U, Schwarz K (2003) Mechanism and regulation of human non-homologous DNA end-joining. *Nat Rev Mol Cell Biol* 4: 712 – 720
4. San Filippo J, Sung P, Klein H (2008) Mechanism of eukaryotic homologous recombination. *Annu Rev Biochem* 77: 229 – 257
5. Branzei D, Foiani M (2008) Regulation of DNA repair throughout the cell cycle. *Nat Rev Mol Cell Biol* 9: 297 – 308
6. Daley JM, Sung P (2014) 53BP1, BRCA1, and the choice between recombination and end joining at DNA double-strand breaks. *Mol Cell Biol* 34: 1380
7. Yun MH, Hiom K (2009) CtIP-BRCA1 modulates the choice of DNA double-strand-break repair pathway throughout the cell cycle. *Nature* 459: 460 – 463
8. Bunting SF, Callen E, Wong N, Chen HT, Polato F, Gunn A, Bothmer A, Feldhahn N, Fernandez-Capetillo O, Cao L *et al* (2010) 53BP1 inhibits homologous recombination in Brca1-deficient cells by blocking resection of DNA breaks. *Cell* 141: 243 – 254
9. Bothmer A, Robbiani DF, Feldhahn N, Gazumyan A, Nussenzweig A, Nussenzweig MC (2010) 53BP1 regulates DNA resection and the choice between classical and alternative end joining during class switch recombination. *J Exp Med* 207: 855 – 865
10. Panier S, Boulton SJ (2014) Double-strand break repair: 53BP1 comes into focus. *Nat Rev Mol Cell Biol* 15: 7 – 18
11. Poulsen M, Lukas C, Lukas J, Bekkerjensen S, Mailand N (2012) Human RNF169 is a negative regulator of the ubiquitin-dependent response to DNA double-strand breaks. *J Cell Biol* 197: 189 – 199

12. Kitevski-LeBlanc J, Fradet-Turcotte A, Kukic P, Wilson MD, Portella G, Yuwen T, Panier S, Duan S, Canny MD, van Ingen H *et al* (2017) The RNF168 paralog RNF169 defines a new class of ubiquitylated histone reader involved in the response to DNA damage. *Elife* 6: e23872
13. Hu Q, Botuyan MV, Cui G, Zhao D, Mer G (2017) Mechanisms of ubiquitin-nucleosome recognition and regulation of 53BP1 chromatin recruitment by RNF168/169 and RAD18. *Mol Cell* 66: 473 – 487 e9
14. Levine AJ, Momand J, Finlay CA (1991) The p53 tumour suppressor gene. *Nature* 351: 453 – 456
15. Hollstein M, Sidransky D, Vogelstein B, Harris CC (1991) p53 mutations in human cancers. *Science* 253: 49 – 53
16. Riley T, Sontag E, Chen P, Levine A (2008) Transcriptional control of human p53-regulated genes. *Nat Rev Mol Cell Biol* 9: 402 – 412
17. Huarte M, Guttman M, Feldser D, Garber M, Koziol MJ, Kenzelmann-Broz D, Khalil AM, Zuk O, Amit I, Rabani M *et al* (2010) A large intergenic noncoding RNA induced by p53 mediates global gene repression in the p53 response. *Cell* 142: 409 – 419
18. Hung T, Wang Y, Lin MF, Koegel AK, Kotake Y, Grant GD, Horlings HM, Shah N, Umbricht C, Wang P *et al* (2011) Extensive and coordinated transcription of noncoding RNAs within cell-cycle promoters. *Nat Genet* 43: 621 – 629
19. Marin-Bejar O, Marchese FP, Athie A, Sanchez Y, Gonzalez J, Segura V, Huang L, Moreno I, Navarro A, Monzo M *et al* (2013) Pint lincRNA connects the p53 pathway with epigenetic silencing by the Polycomb repressive complex 2. *Genome Biol* 14: R104
20. Bertrand P, Saintigny Y, Lopez BS (2004) p53's double life: transactivation-independent repression of homologous recombination. *Trends Genet* 20: 235 – 243
21. Tutt A, Bertwistle D, Valentine J, Gabriel A, Swift S, Ross G, Griffin C, Thacker J, Ashworth A (2001) Mutation in Brca2 stimulates error-prone homology-directed repair of DNA double-strand breaks occurring between repeated sequences. *EMBO J* 20: 4704 – 4716
22. Richardson C, Stark JM, Ommundsen M, Jasin M (2004) Rad51 overexpression promotes alternative double-strand break repair pathways and genome instability. *Oncogene* 23: 546 – 553
23. Liu G, Parant JM, Lang G, Chau P, Chavez-Reyes A, El-Naggar AK, Multani A, Chang S, Lozano G (2004) Chromosome stability, in the absence of apoptosis, is critical for suppression of tumorigenesis in Trp53 mutant mice. *Nat Genet* 36: 63 – 68
24. Linke SP, Sengupta S, Khabie N, Jeffries BA, Buchhop S, Miska S, Henning W, Pedeux R, Wang XW, Hofseth LJ *et al* (2003) p53 interacts with hRAD51 and hRAD54, and directly modulates homologous recombination. *Can Res* 63: 2596 – 2605
25. Sturzbecher HW, Donzelmann B, Henning W, Knippschild U, Buchhop S (1996) p53 is linked directly to homologous recombination processes via RAD51/RecA protein interaction. *EMBO J* 15: 1992 – 2002
26. Dutta A, Ruppert JM, Aster JC, Winchester E (1993) Inhibition of DNA replication factor RPA by p53. *Nature* 365: 79 – 82
27. Arias-Lopez C, Lazaro-Trueba I, Kerr P, Lord CJ, Dexter T, Iravani M, Ashworth A, Silva A (2006) p53 modulates homologous recombination by transcriptional regulation of the RAD51 gene. *EMBO Rep* 7: 219 – 224
28. Prensner JR, Chen W, Iyer MK, Cao Q, Ma T, Han S, Sahu A, Malik R, Wilder-Romans K, Navone N *et al* (2014) PCAT-1, a long noncoding RNA, regulates BRCA2 and controls homologous recombination in cancer. *Can Res* 74: 1651 – 1660
29. Sharma V, Khurana S, Kubben N, Abdelmohsen K, Oberdoerffer P, Gorospe M, Misteli T (2015) A BRCA1-interacting lncRNA regulates homologous recombination. *EMBO Rep* 16: 1520 – 1534
30. Shen L, Wang Q, Liu R, Chen Z, Zhang X, Zhou P, Wang Z (2018) LncRNA lnc-RI regulates homologous recombination repair of DNA double-strand breaks by stabilizing RAD51 mRNA as a competitive endogenous RNA. *Nucleic Acids Res* 46: 717 – 729
31. Lander ES, Linton LM, Birren B, Nusbaum C, Zody MC, Baldwin J, Devon K, Dewar K, Doyle M, FitzHugh W *et al* (2001) Initial sequencing and analysis of the human genome. *Nature* 409: 860 – 921
32. Henikoff S, Greene EA, Pietrokovski S, Bork P, Attwood TK, Hood L (1997) Gene families: the taxonomy of protein paralogs and chimeras. *Science* 278: 609 – 614
33. Thornburg BG, Gotea V, Makalowski W (2006) Transposable elements as a significant source of transcription regulating signals. *Gene* 365: 104 – 110
34. Mourier T, Willerslev E (2009) Retrotransposons and non-protein coding RNAs. *Brief Funct Genomic Proteomic* 8: 493 – 501
35. Cohen CJ, Lock WM, Mager DL (2009) Endogenous retroviral LTRs as promoters for human genes: a critical assessment. *Gene* 448: 105 – 114
36. Wang T, Zeng J, Lowe CB, Sellers RG, Salama SR, Yang M, Burgess SM, Brachmann RK, Haussler D (2007) Species-specific endogenous retroviruses shape the transcriptional network of the human tumor suppressor protein p53. *Proc Natl Acad Sci USA* 104: 18613 – 18618
37. Hu T, Pi W, Zhu X, Yu M, Ha H, Shi H, Choi JH, Tuan D (2017) Long noncoding RNAs transcribed by ERV-9 LTR retrotransposon act in cis to modulate long-range LTR enhancer function. *Nucleic Acids Res* 45: 4479 – 4492
38. Pi W, Zhu X, Wu M, Wang Y, Fulzele S, Eroglu A, Ling J, Tuan D (2010) Long-range function of an intergenic retrotransposon. *Proc Natl Acad Sci USA* 107: 12992 – 12997
39. Zhang H, Zhu C, Zhao Y, Li M, Wu L, Yang X, Wan X, Wang A, Zhang MQ, Sang X *et al* (2015) Long non-coding RNA expression profiles of hepatitis C virus-related dysplasia and hepatocellular carcinoma. *Oncotarget* 6: 43770 – 43778
40. Li XL, Subramanian M, Jones MF, Chaudhary R, Singh DK, Zong X, Gryder B, Sindri S, Mo M, Schetter A *et al* (2017) Long noncoding RNA PURPL suppresses basal p53 levels and promotes tumorigenicity in colorectal cancer. *Cell Rep* 20: 2408 – 2423
41. Ling J, Pi W, Bollag R, Zeng S, Keskintepe M, Saliman H, Krantz S, Whitney B, Tuan D (2002) The solitary long terminal repeats of ERV-9 endogenous retrovirus are conserved during primate evolution and possess enhancer activities in embryonic and hematopoietic cells. *J Virol* 76: 2410 – 2423
42. Zhou KR, Liu S, Sun WJ, Zheng LL, Zhou H, Yang JH, Qu LH (2017) ChIPBase v2.0: decoding transcriptional regulatory networks of non-coding RNAs and protein-coding genes from ChIP-seq data. *Nucleic Acids Res* 45: D43 – D50
43. Dalvai M, Mondesert O, Bourdon JC, Ducommun B, Dozier C (2011) Cdc25B is negatively regulated by p53 through Sp1 and NF-Y transcription factors. *Oncogene* 30: 2282 – 2288
44. Jung MS, Yun J, Chae HD, Kim JM, Kim SC, Choi TS, Shin DY (2001) p53 and its homologues, p63 and p73, induce a replicative senescence through inactivation of NF-Y transcription factor. *Oncogene* 20: 5818 – 5825
45. Yun J, Chae HD, Choi TS, Kim EH, Bang YJ, Chung J, Choi KS, Mantovani R, Shin DY (2003) Cdk2-dependent phosphorylation of the NF-Y transcription factor and its involvement in the p53-p21 signaling pathway. *J Biol Chem* 278: 36966 – 36972

46. Chae HD, Yun J, Bang YJ, Shin DY (2004) Cdk2-dependent phosphorylation of the NF-Y transcription factor is essential for the expression of the cell cycle-regulatory genes and cell cycle G1/S and G2/M transitions. *Oncogene* 23: 4084 – 4088
47. Yun UJ, Park HD, Shin DY (2006) p53 prevents immature escaping from cell cycle G2 checkpoint arrest through inhibiting cdk2-dependent NF-Y phosphorylation. *Cancer Res Treat* 38: 224 – 228
48. Chen J, Feng W, Jiang J, Deng Y, Huen MS (2012) Ring finger protein RNF169 antagonizes the ubiquitin-dependent signaling cascade at sites of DNA damage. *J Biol Chem* 287: 27715 – 27722
49. An L, Jiang Y, Ng HH, Man EP, Chen J, Khoo US, Gong Q, Huen MS (2017) Dual-utility NLS drives RNF169-dependent DNA damage responses. *Proc Natl Acad Sci USA* 114: E2872 – E2881
50. Bellucci M, Agostini F, Masin M, Tartaglia GG (2011) Predicting protein associations with long noncoding RNAs. *Nat Methods* 8: 444 – 445
51. Pierce AJ, Johnson RD, Thompson LH, Jasin M (1999) XRCC3 promotes homology-directed repair of DNA damage in mammalian cells. *Genes Dev* 13: 2633 – 2638
52. Panier S (2012) Tandem protein interaction modules organize the ubiquitin-dependent response to DNA double-strand breaks. *Mol Cell* 47: 383 – 395
53. Vogelstein B, Lane D, Levine AJ (2000) Surfing the p53 network. *Nature* 408: 307 – 310
54. Mirza A, Wu Q, Wang L, McClanahan T, Bishop WR, Gheyas F, Ding W, Hutchins B, Hockenberry T, Kirschmeier P *et al* (2003) Global transcriptional program of p53 target genes during the process of apoptosis and cell cycle progression. *Oncogene* 22: 3645 – 3654
55. Boehden GS, Akyuz N, Roemer K, Wiesmuller L (2003) p53 mutated in the transactivation domain retains regulatory functions in homology-directed double-strand break repair. *Oncogene* 22: 4111 – 4117
56. Dudenhoffer C, Kurth M, Janus F, Deppert W, Wiesmuller L (1999) Dissociation of the recombination control and the sequence-specific transactivation function of P53. *Oncogene* 18: 5773 – 5784
57. Fischer M, Quaas M, Steiner L, Engeland K (2016) The p53-p21-DREAM-CDE/CHR pathway regulates G2/M cell cycle genes. *Nucleic Acids Res* 44: 164 – 174
58. Muller GA, Quaas M, Schumann M, Krause E, Padi M, Fischer M, Litovchick L, DeCaprio JA, Engeland K (2012) The CHR promoter element controls cell cycle-dependent gene transcription and binds the DREAM and MMB complexes. *Nucleic Acids Res* 40: 1561 – 1578
59. Hu T, Zhu X, Pi W, Yu M, Shi H, Tuan D (2017) Hypermethylated LTR retrotransposon exhibits enhancer activity. *Epigenetics* 12: 226 – 237
60. Leonova KI, Brodsky L, Lipchick B, Pal M, Novototskaya L, Chenchik AA, Sen GC, Komarova EA, Gudkov AV (2013) p53 cooperates with DNA methylation and a suicidal interferon response to maintain epigenetic silencing of repeats and noncoding RNAs. *Proc Natl Acad Sci USA* 110: E89 – E98
61. Esteve PO, Chin HG, Pradhan S (2005) Human maintenance DNA (cytosine-5)-methyltransferase and p53 modulate expression of p53-repressed promoters. *Proc Natl Acad Sci USA* 102: 1000 – 1005
62. Wang YA, Kamarova Y, Shen KC, Jiang Z, Hahn MJ, Wang Y, Brooks SC (2005) DNA methyltransferase-3a interacts with p53 and represses p53-mediated gene expression. *Cancer Biol Ther* 4: 1138 – 1143
63. Saintigny Y, Lopez BS (2002) Homologous recombination induced by replication inhibition, is stimulated by expression of mutant p53. *Oncogene* 21: 488 – 492
64. Lower R, Lower J, Kurth R (1996) The viruses in all of us: characteristics and biological significance of human endogenous retrovirus sequences. *Proc Natl Acad Sci USA* 93: 5177 – 5184
65. Temin HM (1981) Structure, variation and synthesis of retrovirus long terminal repeat. *Cell* 27: 1 – 3
66. RNA-seq data of HCC samples (2015) GDC Data Portal TCGA-LIHC https://portal.gdc.cancer.gov/projects/TCGA-LIHC. [DATASET]
67. Liao Y, Smyth GK, Shi W (2013) The Subread aligner: fast, accurate and scalable read mapping by seed-and-vote. *Nucleic Acids Res* 41: e108
68. Rahman M, Jackson LK, Johnson WE, Li DY, Bild AH, Piccolo SR (2015) Alternative preprocessing of RNA-sequencing data in The Cancer Genome Atlas leads to improved analysis results. *Bioinformatics* 31: 3666 – 3672
69. Quinlan AR, Hall IM (2010) BEDTools: a flexible suite of utilities for comparing genomic features. *Bioinformatics* 26: 841 – 842
70. Cerami E, Gao J, Dogrusoz U, Gross BE, Sumer SO, Aksoy BA, Jacobsen A, Byrne CJ, Heuer ML, Larsson E *et al* (2012) The cBio cancer genomics portal: an open platform for exploring multidimensional cancer genomics data. *Cancer Discov* 2: 401 – 404
71. Law CW, Chen Y, Shi W, Smyth GK (2014) voom: precision weights unlock linear model analysis tools for RNA-seq read counts. *Genome Biol* 15: R29
72. Huang da W, Sherman BT, Lempicki RA (2009) Systematic and integrative analysis of large gene lists using DAVID bioinformatics resources. *Nat Protoc* 4: 44 – 57
73. Guo YH, Wang LQ, Li B, Xu H, Yang JH, Zheng LS, Yu P, Zhou AD, Zhang Y, Xie SJ *et al* (2016) Wnt/beta-catenin pathway transactivates microRNA-150 that promotes EMT of colorectal cancer cells by suppressing CREB signaling. *Oncotarget* 7: 42513 – 42526
74. Van Nostrand EL, Pratt GA, Shishkin AA, Gelboin-Burkhart C, Fang MY, Sundararaman B, Blue SM, Nguyen TB, Surka C, Elkins K *et al* (2016) Robust transcriptome-wide discovery of RNA-binding protein binding sites with enhanced CLIP (eCLIP). *Nat Methods* 13: 508 – 514
75. Xing YH, Yao RW, Zhang Y, Guo CJ, Jiang S, Xu G, Dong R, Yang L, Chen LL (2017) SLERT regulates DDX21 rings associated with Pol I transcription. *Cell* 169: 664 – 678 e16
76. Richardson C, Moynahan ME, Jasin M (1998) Double-strand break repair by interchromosomal recombination: suppression of chromosomal translocations. *Genes Dev* 12: 3831 – 3842

